JPL Publication 94-24

A Comparative Survey of Current and Proposed Tropospheric Refraction-Delay Models for DSN Radio Metric Data Calibration

J. A. Estefan
O. J. Sovers

October 1994

National Aeronautics and
Space Administration

Jet Propulsion Laboratory
California Institute of Technology
Pasadena, California

The research described in this publication was carried out by the Jet Propulsion Laboratory, California Institute of Technology, under a contract with the National Aeronautics and Space Administration.

ACKNOWLEDGMENTS

The authors would like to thank C. S. Christensen, G. E. Lanyi, H. N. Royden, and T. F. Runge, all of the Jet Propulsion Laboratory, for their valuable input in preparation of this report. Many thanks to C. C. ("George") Chao of The Aerospace Corporation for helping to shed light on the many facets of his pioneering work in this area during his early tenure at JPL, and to A. E. Niell for supplying his new algorithms and source code prior to publication.

ABSTRACT

The standard tropospheric calibration model implemented in the operational Orbit Determination Program is the seasonal model developed by C. C. Chao in the early 1970s. The seasonal model has seen only slight modification since its release, particularly in the format and content of the zenith delay calibrations. Chao's most recent standard mapping tables, which are used to project the zenith delay calibrations along the station-to-spacecraft line of sight, have not been modified since they were first published in late 1972. This report focuses principally on proposed upgrades to the zenith delay mapping process, although modeling improvements to the zenith delay calibration process are also discussed. A number of candidate approximation models for the tropospheric mapping are evaluated, including the semi-analytic mapping function of Lanyi, and the semi-empirical mapping functions of Davis et al. ("CfA-2.2"), of Ifadis (global solution model), of Herring ("MTT"), and of Niell ("NMF"). All of the candidate mapping functions are superior to the Chao standard mapping tables and approximation formulas when evaluated against the current Deep Space Network Mark III intercontinental very long baseline interferometry database.

CONTENTS

Figures

Tables

SECTION 1

INTRODUCTION

An integral part of NASA's Deep Space Network (DSN)-based tracking and navigation system is the collection of ground-based observations, which are used to continuously correct the prediction of a spacecraft's position in time. These observations, made by a global network of DSN radio antennas, consist of radio metric tracking data such as: 1) Doppler, a measure of "frequency change" between the spacecraft and ground station; 2) range, a measure of line-of-sight "distance" between the spacecraft and ground station; and 3) Very Long Baseline Interferometry (VLBI), an interferometric measure of the spacecraft's "angular position" on the plane of the sky. Radio signals that pass through the Earth's atmosphere are sensitive to electrically neutral particles which cause a time delay in the signal, depending on the dielectric constant of the media and path length. Additionally, if the signal does not travel parallel to the density gradient of the atmosphere, it will be subject to atmospheric refraction, causing its path to deviate from a straight line. Geometrical bending of the signal path is greatly intensified in the lower atmosphere, most notably the troposphere, due to the curvature of the air layer near the Earth's surface (see Fig. 1). This so-called "bending effect" is significant at low station-to-spacecraft elevation angles ($< 10^{\circ}$). Consequently, improved modeling techniques for the excess propagation delay due to the neutral atmosphere must be incorporated into the operational navigation software in order to take full advantage of the high-fidelity zenith delay calibrations that are provided by the DSN's Tracking System Analytic Calibration (TSAC) activity, and further, to reduce the effect of elevation-dependent "mapping" errors induced by projecting the calibrated zenith delays along the station-to-spacecraft line of sight. In this report, the refraction and zenith delay effects of the *entire* neutral atmosphere are collectively referred to as the "tropospheric effect."

The tropospheric calibration model currently implemented in the operational Orbit Determination Program (ODP)[1] of the Jet Propulsion Laboratory (JPL) is based in large part on the seasonal model developed by C. C. Chao of the Mariner Mars 1971 (MM '71) TSAC activity [*Chao*, 1974]. Additionally, in past and current planetary missions, two-way radio metric tracking data acquired from Deep Space Stations (DSSs), have frequently been either deleted (cut off) below 10° to 15° elevation angle or artificially "deweighted" by an elevation-dependent empirical weighting function. The weighting function was developed as an attempt to alleviate any modeling errors introduced by the media calibration process. Unfortunately, these *ad hoc* procedures have pre-empted the need to upgrade the media calibration models in the ODP. The argument for eliminating low-elevation data clearly breaks down when differential data types are incorporated into the orbit determination process; relatively low elevation angles ($\sim 6^{\circ}$) must be used in the differential data acquisition process in order to obtain sufficient tracking coverage between co-observing stations on DSN intercontinental baselines. Differential data types such as

[1]The ODP is a large institutional software system used for research and navigation support of flight operations [*Panagiotacopulos et al.*, 1974].

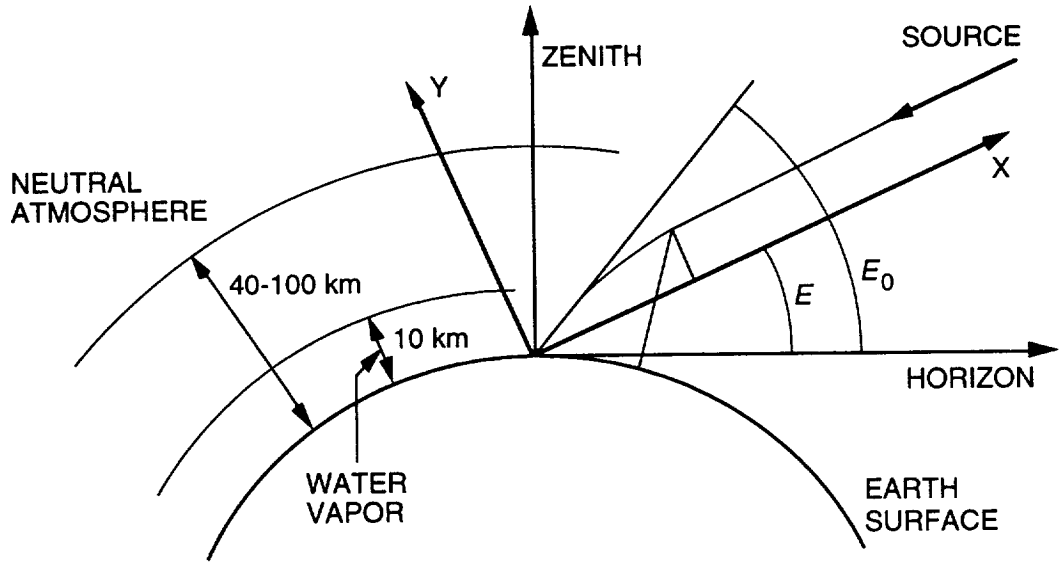

Figure 1. Geometrical bending of the signal path due to tropospheric refraction.

Note: E_0 represents the observed, or "refracted," elevation angle, while E denotes the "unrefracted" (straight-line) elevation angle. (The size of the tropospheric air layer and ray bending are exaggerated for illustration purposes.)

wideband and narrowband VLBI and differenced Doppler and ranging are often used to provide a direct angular measure of the spacecraft on the plane of the sky, as they are typically less sensitive to mismodelings of spacecraft nongravitational forces than conventional two-way radio metric data types.

In Section 2 of this report, the ODP's currently implemented tropospheric calibration model is extensively reviewed. Because this is intended to be an archival document, where appropriate, all relevant mathematical formulations are provided. Section 3 discusses a number of proposed modeling improvements in both the zenith delay calibration and zenith delay mapping processes. Section 4 lays the mathematical framework for a number of candidate tropospheric mapping approximation models, commonly referred to as "tropospheric mapping functions," which has been a very active area of research during the past 2 decades (see *e.g.*, *Gallini* [1994]). Section 5 presents a statistical evaluation of the candidate tropospheric mapping functions based on an extensive set of VLBI measurements acquired at the DSN over a 5 year period extending from 1988 to 1993 using the Mark III data acquisition systems. Section 6 discusses general selection criteria and implementation issues of the candidate mapping functions. Section 7 concludes the report with a general summary statement and specific recommendations for modernizing the tropospheric calibration model in the ODP.

SECTION 2

REVIEW OF THE CURRENT MODEL

An excellent discussion of the transition from early ODP tropospheric calibration models to the currently implemented seasonal model is given by *Mottinger* [1984]. There have been a few changes to the standard model since the time of Mottinger's report, which are documented here along with a review of the current implementation process. In the ODP, the seasonal tropospheric calibration model comprises two fundamental parts: 1) one-way range zenith delay calibrations, or "adjusts," supplied by TSAC in the form of coefficients of a normalized polynomial or Fourier series in time, and 2) standard mapping tables, which are used to project the zenith range correction to the direction of the source, as viewed by the observer. The source can be any spacecraft or extragalactic radio source (EGRS), *i.e.*, quasar, and the observer can be any DSS. A compact formula is then used to compute the actual range tropospheric correction along the line of sight and convert the result to appropriate units, consistent with the data type being used (*e.g.*, Doppler, range, VLBI). This entire process is handled in the program link EDIT independently from the light-time determination and observable formulation, which is performed in the program link REGRES (see Fig. 2) [*Ekelund*, 1993]. The standard implementation makes use of the common practice of separately modeling the hydrostatic, or "dry," component (which comprises atmospheric constituents in hydrostatic equilibrium–principally, N_2, O_2, Ar, and CO_2) from the highly variable water-vapor, or "wet," component. Fortunately, the major contributor to the total delay is the dry component (~90% to ~95%), and its variability at any DSS site is small and seasonal in nature. Typical observed values at the Deep Space Communications Complexes (DSCCs) of DSCC 10 (Goldstone, California), DSCC 40 (Canberra, Australia), and DSCC 60 (Madrid, Spain) for the zenith dry and wet delays are ~200 cm to ~216 cm and ~1 cm to ~25 cm, respectively [*Runge*, 1993].

2.1 Zenith Range Adjusts

The TSAC activity employs a seasonal model to produce calibrations for the zenith dry and wet tropospheric delays and delivers them to flight project navigation teams as coefficients of a normalized polynomial or Fourier series in time. The original seasonal model was derived by Chao in the early 1970s, during which time he studied the influence of seasonal fluctuations in surface meteorological measurements on refractivity, based on radiosonde balloon measurements acquired over a 2 year period (1967 and 1968) from six globally distributed weather stations [*Chao*, 1971]. Chao concluded that the refractivity profiles repeated satisfactorily over the 2 year period and that monthly averages of surface measurements of four meteorological parameters, *i.e.*, surface barometric pressure, P_0, linearly extrapolated temperature, T_0, temperature lapse rate (altitude temperature gradient), w, and surface relative humidity, $(RH)_0$, could be used to predict the zenith dry and wet one-way range delays within a reasonable degree of accuracy, provided that corrections were made to P_0 and T_0 to account for any station altitude offset between the radiosonde station and the nearest DSS. Zenith delay calibrations were determined from polyno-

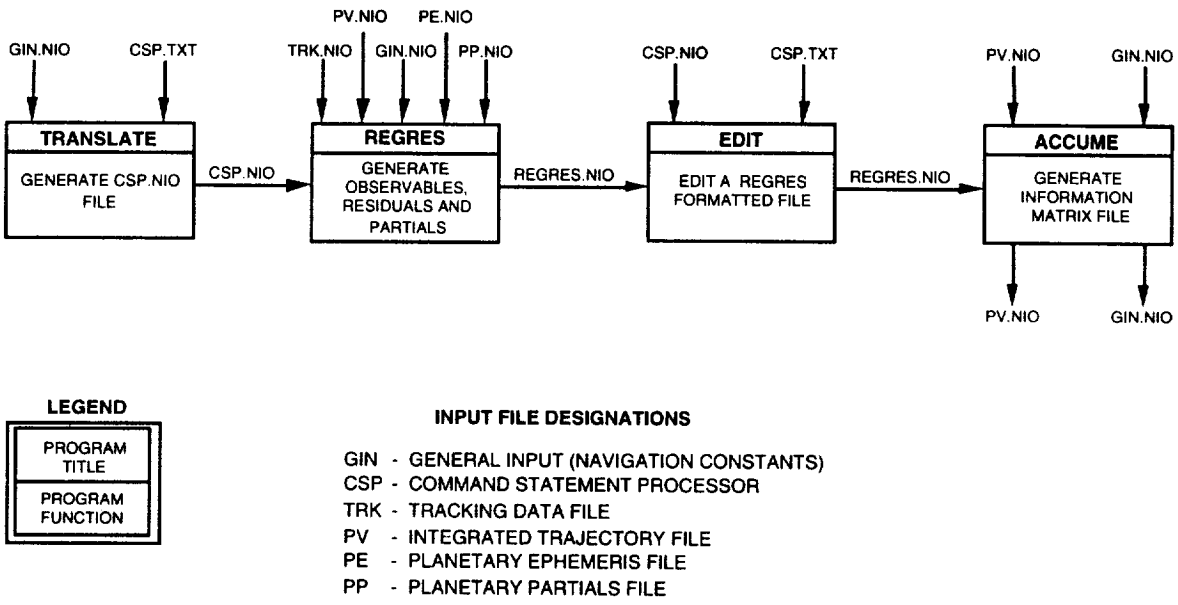

Figure 2. ODP software set functional diagram for observable generation, data editing, and accumulation of the information matrix.

Note: The program links that contain the media models reside in program links REGRES and EDIT. Also shown are the ODP input/output file interfaces. The file extension .NIO represent direct access, binary NAVigation Input-Output (NAVIO) files, while the file extension .TXT represents text-based input files, generally assumed to be Fortran NAMELIST files.

mial fits to zenith delay values computed from monthly averages of surface meteorological measurements using the "Berman 70" model [*Berman*, 1970], which was derived under the assumption of static equilibrium, perfect gas law for the troposphere, and constant gravitational acceleration:

$$\Delta\rho_{Z_{dry}} = 10^{-3} C_1 \left(\frac{R_d}{g}\right) P_0 \tag{1}$$

$$\Delta\rho_{Z_{wet}} = 10^{-3} \left[\frac{C_1 C_2 (RH)_0}{w}\right] \left[\frac{\left(1 - \frac{C}{T_0}\right)^2}{B - AC}\right] \exp\left(\frac{AT_0 - B}{T_0 - C}\right) \tag{2}$$

where

$\Delta\rho_Z$ = zenith range correction, m

P_0 = surface barometric pressure, mbar (1 mbar = 10^2 N/m^2)

w = temperature lapse rate, K/km

T_0 = linearly extrapolated surface temperature, K

$(RH)_0$ = surface relative humidity ($0 \le (RH)_0 \le 1$)

A = 17.1485

B = 4684.1

C = 38.45

g = gravitational acceleration, 980.6 cm/s^2

R_d = perfect gas constant of dry air, 0.287 J/g•K

g/R_d = 34.1 K/km

C_1 = 77.6

C_2 = 29341.0

In the seasonal model, monthly means of $(RH)_0$ were averaged over each month to overcome the inadequacy of Eq. (2) to possible fluctuations in relative humidity with altitude. This model was adopted as the standard zenith delay tropospheric calibration method for MM'71 [*Chao*, 1974].

Although the format and content of the TSAC tropospheric calibration polynomials has evolved over the years, they are still delivered as "card images" which conform to the Command Statement Processor (CSP) English-like command language used by the ODP to adjust, delete, or weight data points.[2] In general, a CSP command consists of a verb and optional scope limiters and computation specifiers, terminated by a period [*DPTRAJ-ODP User's Reference Manual, Vol. 1, Rev. F*, 1994]. A command may, and frequently does, extend over more than one card image. Elements of CSP commands used in the TSAC media calibrations are summarized in Table 1.

The ADJUST command for media calibrations takes the general form

ADJUST (data-type)	BY SERIES-TYPE (coefficients)	
MODEL (model-name)	FROM (A) TO (B)	DSN (complex)

Additional explanatory information, not to be used in the actual adjustment process, may appear on a command provided that it is preceded by a number sign (#). The ADJUST (data-type) command verb indicates that the calibrations were derived especially for a specific class of data types. The allowable options for the data-type argument are ALL (corrections to be applied to all data types), DOPRNG (Doppler and range), or VLBI (exclusively).

Media calibrations may be specified by a normalized power series (NRMPOW), a Fourier series (TRIG), or in special cases, by a single constant (CONST). In the past, the coefficients or the constant could be represented as single- or double-precision floating-point numbers with the computation specifier preceded by the letter "D" for the double-precision format (*e.g.*, DNRMPOW). This level of precision has since been determined to be unnecessary, hence, all

[2] A detailed description of the format and content of TSAC media calibrations is given in *DSN Tracking System Interfaces, Media Calibration Interface (TRK-2-23)* [1985]. Excerpts from that document are given here for completeness and include recent undocumented modifications and enhancements.

coefficients or constants are provided as single-precision floating point numbers accurate to four decimal places [*Royden*, 1994].

Table 1. Command Statement Processor (CSP) elements used in TSAC media calibrations.

Type of Element	Elements Used
Verbs	ADJUST, DELETE
Scope Limiters	Time Span Limiters: FROM BEFORE TO AFTER AT Network (Complex or Station): DSN C10 (Goldstone) 11, 12, . . . , 19 C40 (Australia) 41, 42, . . . , 49 C60 (Spain) 61, 62, . . . , 69 Band: S, X Source: SCID, QUASAR
Computation Specifier	Series Type: BY NRMPOW BY CONST BY TRIG Model: DRY NUPART (dry troposphere) WET NUPART (tropospheric water vapor) CHPART (ionosphere) DRVID (ionosphere + solar plasma)[a] Data Type: ALL DOPRNG VLBI
	[a]obsolete

For tropospheric calibrations, the MODEL (model-name) computation specifier takes the form of either MODEL (DRY NUPART) or MODEL (WET NUPART), depending on whether dry or wet zenith tropospheric delay calibrations are to be calculated from the polynomial coefficients supplied. Series representation of the zenith range adjusts are determined as follows: Let T be the time associated with the current data point. For the BY SERIES (C_0, C_1, ..., C_n)

FROM (A) TO (B) part of the ADJUST command, the zenith range adjust, $\Delta\rho_Z$, is computed from one of the following series types:

- Normalized power series (BY NRMPOW)

$$\Delta\rho_Z = \sum_{k=0}^{n} C_k X^k \tag{3}$$

This is referred to as a "normalized" power series because the time argument of the series, T, is replaced by a normalized, dimensionless argument X, which is defined to be -1 when $T = A$ and +1 when $T = B$. The normalization is performed through the change of variable $X = 2((T - A)/(B - A)) - 1$. Currently, TSAC uses a 10th-degree polynomial to perform the fit. Thus, for the standard model, $n = 10$.

- Fourier series (BY TRIG)
Renaming the coefficients as BY TRIG $(P,C,D_1,E_1,D_2,E_2,...,D_n,E_n)$:

$$\Delta\rho_Z = C + \sum_{k=1}^{n} \left[D_k \cos(2\pi k X) + E_k \sin(2\pi k X)\right] \tag{4}$$

where P is the period of the fundamental mode (in seconds) and $X = (T - A) / P$. For the standard model, $n = 4$.

In some cases, an additional adjustment may be given in the form of a simple constant such as a correction for a station altitude offset:

- Constant (BY CONST)

$$\Delta\rho_Z = C_0 \tag{5}$$

The format of the time sequence is taken to be YY/MM/DD,HH,mm,ss.ff, where YY is the last two digits of the year, MM is the number of the month, DD is the day of the month, HH is the hour, mm is the minute and ss.ff the seconds and fractional part of a second, respectively. Up to three of the right-most time fields may be omitted. When omitted, their default values are taken to be zeros.

The dry and wet adjust cards are repeated pairwise as necessary to cover all DSCCs from which radio metric tracking data are expected. These are denoted by the scope limiters DSN (C10), DSN (C40), and DSN (C60). Two examples of tropospheric adjust card image streams are shown in Figs. 3a and 3b and are representative of the "official" seasonal model. Illustrated are the 10th-degree normalized power series representation (NRMPOW) and 4th-degree Fourier

```
 # DSN TROPOSPHERE CALIBRATIONS FROM 89/1/1 TO 91/1/1
 # FOR MAGELLAN ODP
 #
ADJUST (ALL) BY NRMPOW (  0.0539,   -0.1545,    0.6120,    0.8394,   -1.7571,
  -1.1924,    1.7748,   0.6266, -0.7482, -0.1117,  0.1137) MODEL (WET NUPART)
 FROM (89/1/1,00:00:00.01) TO (91/1/1) DSN (C10).

ADJUST (ALL) BY NRMPOW (  2.0601,    0.0000,   -0.1453,   -0.0003,    0.4194,
  -0.0010,   -0.4272,   0.0029,   0.1822, -0.0014, -0.0281) MODEL (DRY NUPART)
 FROM (89/1/1,00:00:00.01) TO (91/1/1) DSN (C10).

ADJUST (ALL) BY NRMPOW (  0.1393,    0.0148,   -0.4576,   -0.0854,    1.3414,
    0.1292,  -1.3936,  -0.0714,   0.6081,   0.0131, -0.0961) MODEL (WET NUPART)
 FROM (89/1/1,00:00:00.01) TO (91/1/1) DSN (C40).

ADJUST (ALL) BY NRMPOW (  2.1541,   -0.0013,    0.0777,    0.0063,   -0.2608,
  -0.0077,    0.3180,   0.0032, -0.1643, -0.0004,  0.0305) MODEL (DRY NUPART)
 FROM (89/1/1,00:00:00.01) TO (91/1/1) DSN (C40).

ADJUST (ALL) BY NRMPOW (  0.0986,   -0.1422,    0.4960,    0.7966,   -1.4194,
  -1.1690,    1.4176,   0.6323, -0.5845, -0.1150,  0.0858) MODEL (WET NUPART)
 FROM (89/1/1,00:00:00.01) TO (91/1/1) DSN (C60).

ADJUST (ALL) BY NRMPOW (  2.1128,   -0.0014,   -0.0614,    0.0021,    0.1593
    0.0076,  -0.1330,  -0.0108,   0.0392,   0.0033, -0.0026) MODEL (DRY NUPART)
 FROM (89/1/1,00:00:00.01) TO (91/1/1) DSN (C60).
#
```

Figure 3a. Format of the TSAC-supplied zenith delay tropospheric calibrations for the "official" seasonal model given as a 10th-degree normalized polynomial.

Note: Sample time span from the Magellan mission.

series representation (TRIG), respectively. Either one of these representations can be used for operational orbit determination; however, the latter has been shown to give a better characterization of the fitted data [*Royden*, 1994]. A further advantage of the TRIG representation is that the user does not need to change the time sequence for which the tropospheric corrections are to be applied, as is currently required in the NRMPOW case (which only covers a 2 year span).

In the ODP, all ADJUST commands compute a correction which is subtracted from the REGRES-generated observed-minus-computed (O-C) residual (resulting in a positive correction to the computed observable). Hence, TSAC media calibrations will always be positive, *i.e.*, a positive sign corresponds to a one-way range delay.

2.2 Standard Mapping Tables

Once the zenith range adjust has been accurately determined, it must be projected, or "mapped," to the line of sight along the observer-to-radio source direction. In the ODP, standard tables of normalized scale factors are used for mapping the zenith range adjusts down to a given

```
ADJUST(DOPRNG)BY TRIG(31557600.,   0.0870,   -0.0360,   -0.0336,    0.0002,
   0.0200,    0.0008,  -0.0021,  -0.0036,   -0.0002)
MODEL
(WET NUPART)FROM(72/01/01,00:00)                    DSN(C10).     #ADJ 920121
02:23
ADJUST(DOPRNG)BY TRIG(31557600.,   2.0521,    0.0082,   -0.0005,   -0.0004,
   0.0033,   -0.0015,   0.0005,  -0.0011,    0.0036)
MODEL
(DRY NUPART)FROM(72/01/01,00:00)                    DSN(C10).     #ADJ 920121
02:23
ADJUST(DOPRNG)BY TRIG(31557600.,   0.1149,    0.0255,    0.0020,    0.0010,
   0.0026,    0.0036,  -0.0001,   0.0007,    0.0012)
MODEL
(WET NUPART)FROM(72/01/01,00:00)                    DSN(C40).     #ADJ 920116
03:35
ADJUST(DOPRNG)BY TRIG(31557600.,   2.1579,   -0.0032,   -0.0002,    0.0012,
   0.0017,   -0.0043,   0.0052,   0.0016,   -0.0021)
MODEL
(DRY NUPART)FROM(72/01/01,00:00)                    DSN(C40).     #ADJ 920116
03:35
ADJUST(DOPRNG)BY TRIG(31557600.,   0.1255,   -0.0284,   -0.0273,   -0.0094,
   0.0005,   -0.0031,  -0.0003,  -0.0034,   -0.0013)
MODEL
(WET NUPART)FROM(72/01/01,00:00)                    DSN(C60).     #ADJ 920116
03:38
ADJUST(DOPRNG)BY TRIG(31557600.,   2.1094,    0.0037,   -0.0010,    0.0036,
   0.0019,   -0.0006,   0.0021,   0.0018,   -0.0004)
MODEL
(DRY NUPART)FROM(72/01/01,00:00)                    DSN(C60).     #ADJ 920116
03:38
```

Figure 3b. Format of the TSAC-supplied zenith delay tropospheric calibrations for the "official" seasonal model given as a 4th-degree Fourier series.

unrefracted (straight-line) elevation angle, E, of a particular leg of the signal path between the observer (transmitting or receiving station) and the source (spacecraft or quasar). Separate tables are used for mapping the zenith dry and wet range corrections with values given at intervals of 0.1° for elevation angles between 0 and 10°, and at intervals of 0.5° for elevation angles between 10° and 90°. Intermediate values not given in the table are determined by the following quadratic interpolation scheme:

$$R(E) = R_i + n\,(R_{i+1}-R_i) + \frac{1}{2}\,n\,(n-1)\left[(R_{i+1}-R_i) - (R_i-R_{i-1})\right] \qquad (6)$$

where

$R(E)$ = mapping factor interpolated from the standard dry or wet table

E = $E_i + \Delta E$, a given elevation angle, $E_i \le E < E_{i+1}$

n = $\dfrac{\Delta E}{E_{i+1} - E_i}$

The frequency of values given in the mapping tables is claimed to limit the error introduced by the interpolation to less than 0.1% of the total tropospheric effect [*Ondrasik*, 1970].

The mapping tables currently in use were derived from ray trace results based on best-fit refractivity profiles from Chao's examination of the 1967 and 1968 radiosonde balloon data described earlier [*Chao*, 1971], and normalized by the ray-traced zenith range correction. The ray tracing algorithm that Chao used to compute the tabular values is described in *Chao* [1972a], and in greater detail in *Miller et al.* [1971]. These mapping tables take into account the geometrical bending effect of the signal path, which becomes significant at low elevation angles [*Chao*, 1972b]. (It should be noted that these "modified" tables were first used operationally to support the Mariner-Venus-Mercury 1973 (MVM'73) mission and superseded the original mapping tables used for MM'71, which did not include the bending effect [*Mottinger*, 1984].) Although there are provisions in the ODP for overriding these tables, stored as vector arrays "TABDRY" and "TABWET," the modified Chao tables have been handed down from flight project to flight project over the years and are still in operational use today. A standard file convention for the improved mapping tables was adopted in 1977 to support the Voyager mission (and every planetary mission since) and is provided in the Appendix. These tables are used by program link EDIT to compute the actual tropospheric mapping corrections.

For use in approximate analysis, the mapping tables and quadratic interpolation algorithm were found to be somewhat cumbersome to implement and not readily portable to different computer platforms. In the development of a simple approximation model to perform the mapping, Chao recognized that a flat Earth model such as $R(E) = 1/\sin E$ would be inadequate, particularly at low elevation angles. Therefore, he extended the flat Earth approximation in a two-term continued fraction which could more accurately perform the dry and wet mapping:

$$R_i(E) = \frac{1}{\sin E + \dfrac{A_i}{\tan E + B_i}} \tag{7}$$

where, for i = dry:

$$\begin{aligned} A_{\text{dry}} &= 0.00143 \\ B_{\text{dry}} &= 0.0445 \end{aligned} \tag{8a}$$

and, for i = wet:

$$\begin{aligned} A_{\text{wet}} &= 0.00035 \\ B_{\text{wet}} &= 0.017 \end{aligned} \tag{8b}$$

The mapping coefficients, A_i and B_i, were derived from empirical fits to the *original* ray trace results. First evidence of Chao's two-term continued fraction form of the dry mapping function [Eqs. (7) and (8a)] can be found in an internal document published in late 1970 [*Chao*, 1970]. The tan E term in the continued fraction was intended to be a normalization factor in order to

ensure that the mapping ratio would numerically approach unity at zenith, *i.e.*, $R(90°) = 1$. Chao determined that the semi-empirical model was good to within 1% from the ray trace range correction for an elevation angle higher than 1°. It is this formula which is used to compute the parameter partial derivatives (partials) in the ODP [*Moyer*, 1984], and which is frequently referenced throughout the literature. Until about 10 years ago, Chao's semi-empirical mapping function was arguably the simplest and most widely used closed form mapping function for any range of elevation angles.

2.3 Creating the Line-of-Sight Tropospheric Correction

A concise formula is used to determine the dry and wet tropospheric corrections (to the computed observable) for any radio metric data type derived from Doppler tracking, ranging, or VLBI techniques, assuming the zenith range adjusts and mapping factors have been adequately determined. This formula, described in detail by *Christensen* [1979a], can be expressed in algorithmic form as

$$\text{TROPOSPHERIC ADJUST} = \sum_{\substack{\text{all} \\ \text{times} \\ \text{(legs)}}} \text{TRPSGN} * \text{UC} * \text{POLY(TIME)} * \text{ELVFAC} \qquad (9)$$

The tropospheric sign factor TRPSGN can be ±1 depending on the direction of the leg (up or down) and the data type being used. The variable UC is the data type unit conversion factor from meters to "correct" units, and POLY(TIME) is any of the legitimate user-selectable ADJUST polynomials in meters of delay, as a function of time; these are generally the tropospheric zenith corrections supplied by TSAC based on the seasonal model. When utilizing the official seasonal model, the user should select the TRIG option (see earlier remarks). The variable ELVFAC is the elevation-angle-dependent mapping factor used to obtain the correction for the true (unrefracted) elevation angle. As described earlier, it is obtained by quadratic interpolation of either the TABWET or TABDRY array with the elevation angle for the appropriate station and time. In general, the selected model correction must be computed at several different times for a given data point, as the tropospheric effect can vary with time. Of note, the only difference between computing the model corrections for the dry versus wet components of the tropospheric effect are in the interpolation tables TABDRY and TABWET used to compute ELVFAC [*Collier*, 1981].

2.4 Artificial Deweighting of Low Elevation Data

Although not officially part of the ODP's tropospheric calibration model, an empirically-derived data editing scheme has been historically used to artificially "deweight" radio metric data acquired at low elevation angles [*Christensen*, 1979b]. The deweighting scheme was originally developed in an attempt to alleviate errors induced by mismodelings of the tropospheric and ionospheric corrections, but optimized for 2.3 GHz (S-band) data. Alternative data weighting

algorithms for 8.4-GHz (X-band) and 32-GHz (Ka-band) Doppler data have been investigated by *Ulvestad and Thurman* [1992] and by *Ulvestad* [1992]. Although better optimized for these higher link frequencies, these algorithms have yet to be incorporated into the operational ODP.

The additional data editing process, as with the tropospheric (and ionospheric) corrections, is handled by the program link EDIT, and invoked with the CSP command

WEIGHT (data-type) SIGMA (S)

where S denotes the 1-sigma measurement uncertainty associated with a given data point. The data-type argument can be any of the allowable data types supported by the ODP, *e.g.*, radio metric, angle, or optical [*DPTRAJ-ODP User's Reference Manual, Vol. 1, Rev. F*, 1994]. Let σ_i represent the input "uncorrected" measurement uncertainty S, associated with the ith data point, and let $\bar{\sigma}_i$ denote the associated "corrected" sigma. For the elevation-dependent radio metric data of Doppler, range, and VLBI, the weighting algorithm is given by

$$WEIGHT = \frac{1}{\bar{\sigma}_i^2} \tag{10}$$

where

$$\bar{\sigma}_i = \sigma_i * E * F \tag{11}$$

Here,

$E = 1 + \dfrac{18}{(E_{min_i} + 1)^2}$

E_{min_i} = minimum elevation angle (in degrees) associated with the ith data point

$F = \sqrt{\dfrac{60}{TC_i}}$

TC_i = count time (in seconds) assigned to the ith data point

The count time factor, F, is to be applied to Doppler and narrowband VLBI; for range and wideband VLBI, F is taken to be unity. Again, variations on this weighting scheme for application to other elevation-dependent radio metric and non-radio metric data types are described in *DPTRAJ-ODP User's Reference Manual, Vol. 1, Rev. F* [1994].

SECTION 3

PROPOSED MODEL IMPROVEMENTS

As seen from the previous discussion, the ODP infrastructure for computing tropospheric corrections is non-trivial, a result largely of early interface design requirements. Ideally, tropospheric and other media calibrations should be applied directly to the computed observables and parameter partials during the light time solution. In this way, no post-production data editing would be required and future modeling upgrades could easily be incorporated into the standard model [*Collier*, 1993]. Unfortunately, a complete redesign of the ODP's media calibration process does not appear fiscally realizable, at least not in the foreseeable future. Nevertheless, there are still improvements which can be incorporated into the current infrastructure, specifically, with respect to the fidelity of the TSAC-supplied zenith delay calibrations, and to the zenith delay mapping process. The proposed model improvements presented herein could be made with modest resource requirements and in a relatively short period of time.

3.1 Zenith Delay Calibrations

The TSAC software has the capability to apply real-time surface meteorological data to further improve the seasonal model if such a need is warranted [*Runge*, 1993], subject to the quality of the instruments used at the DSN. When surface data are used, the residuals (surface model minus seasonal model) can be fit with a polynomial of degree up to 9 or a Fourier series with degree up to 4. The real-time zenith dry delay calibration is based on a modified form of the dry component of the *Saastamoinen* [1972] model, which accounts for the site variability of gravity:

$$\Delta\rho_{Z_{dry}}\,(\mathrm{m}) \;=\; 0.0022768\frac{P_0}{f(\varphi, H_s)} \tag{12}$$

where

$$f(\varphi, H_s) \;=\; 1 - 0.00266\cos 2\varphi - 0.00000028\,H_s \tag{13}$$

Here, φ is the geodetic latitude of the DSS in degrees and H_s the station mean sea level (MSL) height (*i.e.*, height above the reference ellipsoid) in meters. Recall that P_0 is the surface barometric pressure measured in millibars.

This is a significant improvement over the seasonal model in that it relaxes the assumption of constant gravitational acceleration assumed by the Berman 70 model. In addition, this model was derived using the refractivity constants of *Thayer* [1974] which supersede the obsolete values used by Saastamoinen and Berman. A more detailed discussion and derivation is given by *Davis et al.* [1985] and *Elgered* [1993].

It is important to note that Eqs. (12) and (13) model the zenith dry delay at the location of the barometer, therefore, an additional adjustment of the dry delay calibration must be made to the altitude of the local DSS. The following adjustment model performs that function and utilizes average surface pressure and temperature values measured at each DSCC:

$$\Delta\rho_{Z_{dry}}\ (\mathrm{m}) = -0.0000776\left(\frac{P_{avg}}{T_{avg}}\right)\Delta H_S \tag{14}$$

This altitude adjustment model was derived from a simple application of the hydrostatic equation and perfect gas law [*Runge*, 1993]. The altitude correction, ΔH_S, is simply the altitude offset between the local DSS and the reference location of the 70-m antennas at each respective DSCC. The major sources of zenith dry delay errors and their magnitudes are summarized below in Table 2 for both normal and extreme wind conditions.

Table 2. Major sources of zenith dry delay errors under normal and extreme wind conditions.

Error Source	Zenith Dry Delay Errors (mm) Normal	Extreme Wind
Pressure sensor error	2.3	2.3
Uncertainty in physical constants	1.4	1.4
Use of P_{avg}/T_{avg} for 100 m ΔH_S	0.8	0.8
2-m error in ΔH_S	0.5	0.5
Lack of hydrostatic equilibrium	0.2	4.0
Total (root-sum-square)	2.9	4.9

For the real-time zenith wet delay calibration, the TSAC software utilizes the *Callahan* [1973] model, given by

$$\Delta\rho_{Z_{wet}}\ (\mathrm{m}) = 1035\,\frac{e_0}{T_0^2} \tag{15}$$

where e_0 is the partial pressure of water vapor at the surface in millibars and T_0 is, as before, the surface temperature in kelvin. Since the TSAC software does not incorporate dew point data, it calculates e_0 based on a variation of the simple model of *Bean and Dutton* [1966]:

$$e_0 = 6.11\,(RH)_0\,10^{7.5(T_0-273.15)/(T_0-35.85)} \tag{16}$$

where $(RH)_0$ is, as defined in Eq. (2), the surface relative humidity, $0 \le (RH)_0 \le 1$. The observed mean of e_0 for the DSN is about 8 mbar [*Runge*, 1993]. There is a provision to utilize the zenith wet delay model of Chao as an option [*Chao*, 1973]; however, the Callahan model is preferred due to its simplicity. Chao's model for the zenith wet delay can be expressed by

$$\Delta\rho_{Z_{wet}}\,(\mathrm{m}) \;=\; 1.63\,\frac{e_0^{1.23}}{T_0^2} + 2.05w\,\frac{e_0^{1.46}}{T_0^3} \tag{17}$$

where w is, as previously defined, the temperature lapse rate in K/km. The sign of w is determined by the linear lapse function $T = T_0 - w(h - h_0)$, whereby the altitude, h, is constrained to lie between the altitude at the surface, h_0, and the altitude where temperature becomes nearly constant as h increases (~10 km).

It is widely known that the wet component of the troposphere is highly variable due to spatial and temporal inhomogeneities in the atmospheric water vapor content. Consequently, the Callahan and Chao models are only accurate to about 30% and correspond to an uncertainty in the wet delay on the order of 6 cm to 10 cm. Investigators have shown that the zenith wet delay model of *Saastamoinen* [1972] gives a modest improvement over both the Callahan and Chao models in certain applications (see *e.g.*, *Ifadis* [1986]). Saastamoinen's model for the zenith wet delay is given by

$$\Delta\rho_{Z_{wet}}\,(\mathrm{m}) \;=\; 0.002277e_0\left(\frac{1255}{T_0} + 0.05\right) \tag{18}$$

A host of other zenith wet delay calibration models have been derived by a number of authors, including *Hopfield* [1971], *Berman* [1976] (in various forms), *Ifadis* [1986], and more recently, *Baby et al.* [1988]. Because the variability of the atmospheric water vapor content is highly dependent on site and season, a universal model for the zenith wet delay has yet to be developed.

Other more esoteric techniques include the use of Water Vapor Radiometers (WVRs), which infer the wet delay from sky brightness temperature measurements [*Winn et al.*, 1976; *Resch*, 1984]. Theoretically, WVRs can not only accurately predict the zenith wet delay, but the entire wet tropospheric effect along the line of sight [*Davis et al.*, 1985; *Wilcox*, 1992]. Unfortunately, the WVR instruments have proven to be expensive and unreliable (see study by *Elgered et al.* [1991]).

The most promising approach to determining the wet component of the zenith delay appears to be estimating it along with the radio metric tracking data. This has been demonstrated successfully using space-based geodetic systems such as VLBI and the Global Positioning System (GPS) [*Herring et al.*, 1990; *Tralli and Lichten*, 1990]. A comparison of estimates determined from both systems was recently published by *Tralli et al.* [1992]. The TSAC activity is currently studying the feasibility of incorporating GPS-based measurements into the zenith wet tropospheric delay calibration process [*Runge*, 1994]. Although not yet approved for operational use, the GPS technique treats the "total" zenith delay as a nuisance parameter in the data estimation process, and has yielded estimates of the zenith tropospheric delay to better than 1 cm in recent demonstrations [*Lichten*, 1994]. The current TSAC plan is to obtain the time series of the GPS-derived total zenith delays over the time span of interest, and then extract the wet component from the total delay by simply subtracting the dry component determined from real-

time surface barometric pressure measurements. An actual data demonstration of this technique is currently being devised.

3.2 Mapping Phase

It is important to note that the standard mapping tables used in the ODP represent a "snapshot" of the refractivity profiles for a specific set of sites and seasons. Additionally, there is no provision in Chao's semi-empirical mapping formula for utilizing surface weather data at a particular DSS site. Rigorously speaking, a new set of tables, and therefore a new "fitted" mapping function, should be issued for a different refractivity profile [*Chao*, 1972a]. Furthermore, Chao's ray tracing computer programs, used to generate the ODP mapping tables, were re-examined by *Lanyi* [1983]. Lanyi found that while the ray tracing algorithm was adequate, Chao's assumption of the refractivity profile appeared to contradict the physical model, albeit at a relatively low error level, resulting in about a 2-cm discrepancy at 6° in the modified tables. In addition, a recent more thorough examination of the dry mapping tables revealed a small discrepancy of ~0.5 cm in the 11°-elevation regime between the tabular values and the semi-empirical formula. It is believed that this discrepancy can be attributed to limitations in the original ray tracing quadrature procedure; however, no similar behavior was evident for the corresponding wet mapping table.

Another important observation is that the empirical formula expressed by Eqs. (7) and (8) actually corresponds to the original mapping tables and not to the improved mapping tables. (Recall that the improved mapping tables included the geometrical bending effect.) According to *Chao* [1994], a new set of unpublished empirical constants were derived for the dry component of the delay around the 1977 to 1978 timeframe. The following "revised" constants enabled the dry approximation formula to more closely match the refined tables:

$$\begin{aligned} A_{\text{dry}} &= 0.00147 \\ B_{\text{dry}} &= 0.0400 \end{aligned} \tag{19}$$

A cursory examination of the revised dry mapping function against the current dry mapping table does indeed suggest a marked improvement over the original formula [*cf.*, Eqs. (7) and (8a)]. However, it should be noted that there are certain regions in which the revised mapping function exhibits a greater departure from the refined tables than the original mapping function. This discrepancy is most prominent at the extremely low elevation angles (< 2°), as demonstrated in Fig. 4, and to a lesser extent in regions between 10° and 30° (not shown in the figure). It is important to note that although the revised constants yield improved results over the original constants, the Chao approximation model is still limited by the fact that it cannot be readily adaptable to varying atmospheric conditions.

As indicated in the introductory remarks, the process of mapping zenith tropospheric delay calibrations down to lower elevation angles has been studied extensively in recent years. Much

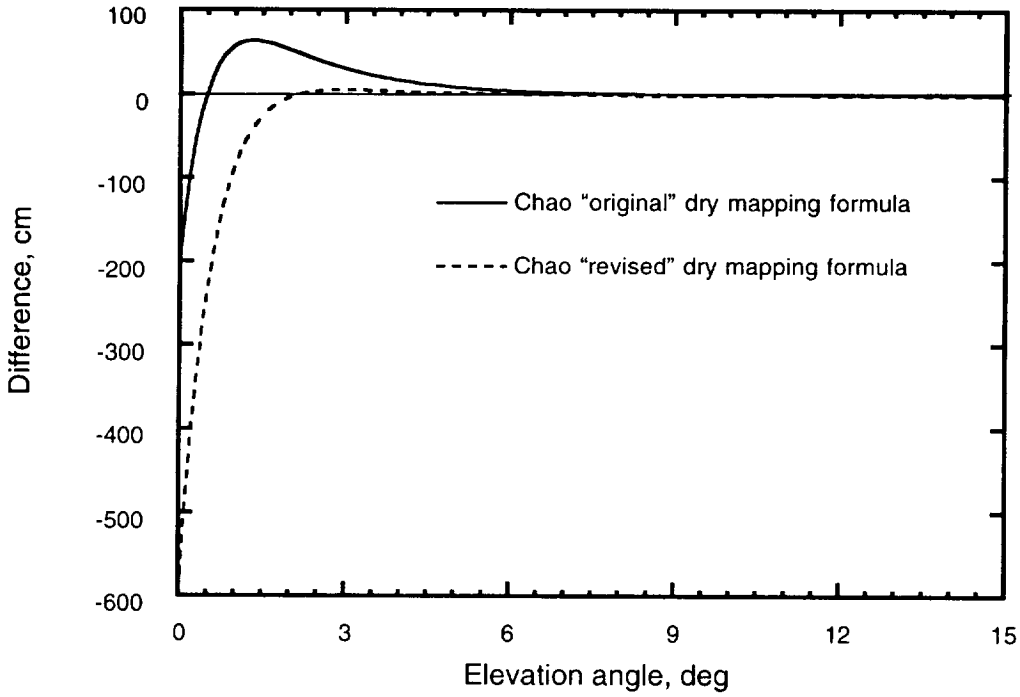

Figure 4. Differences between mapping ratios predicted by Chao's original and revised dry semi-empirical approximation formulas and Chao's improved dry mapping table (TABDRY) at the lower elevation angles.

of the work in this area has come from the VLBI science community, as the refractive and delay effects of the neutral atmosphere effects continue to be a limiting error source in high-precision space-based geodetic analysis. VLBI and other interferometric techniques on long baselines have consistently been plagued by the fact that mutual visibility of either a spacecraft or EGRS between co-observing stations is limited, and therefore requires observations to be taken at relatively low elevation angles [*MacMillan and Ma*, 1994]. This is certainly the case for the long intercontinental baselines of the DSN. The need to acquire interferometric measurements at low elevation angles has the advantage, however, in that such observations help reduce the correlation between estimates of the zenith tropospheric delay and station vertical position. This is arguably the principal reason that radio source observations are being acquired at ever decreasing elevation angles in the space-based geodetic applications.

The remainder of this report is dedicated to assessing a set of modern and robust tropospheric mapping functions intended to replace the outdated Chao tables in the ODP. Although some of these candidate mapping functions accurately model the tropospheric mapping down to as low as 2°, antenna pointing restrictions imposed on the DSSs due to ground obstructions, system noise, and signal multipath usually preclude tracking below 6°. Furthermore, spatial and temporal inhomogeneities in the atmosphere begin to dominate the uncertainty in the overall tropospheric effect in the extremely low elevation regimes (< 5°), and contribute more to the total calibration model uncertainty than simply the zenith delay and/or mapping errors [*Lanyi*, 1984].

SECTION 4

MATHEMATICAL DESCRIPTION OF CANDIDATE MAPPING FUNCTIONS

The simplest way to characterize the one-way range tropospheric correction is in terms of separate dry and wet components:

$$\Delta\rho_{\text{trop}}(E) \equiv \rho_{Z_{\text{dry}}} R_{\text{dry}}(E) + \rho_{Z_{\text{wet}}} R_{\text{wet}}(E) \tag{20}$$

Here, $\rho_{Z_{\text{dry}}}$ and $\rho_{Z_{\text{wet}}}$ are, as before, the range corrections at zenith due to the dry and wet components of the troposphere, respectively. The functions $R_{\text{dry}}(E)$ and $R_{\text{wet}}(E)$ give the ratios for mapping the zenith range corrections down to the given unrefracted elevation angle, E, along the station-to-spacecraft (or EGRS) line of sight. Recall that in the ODP, these ratios, or "mapping factors," are obtained by quadratic interpolation of Chao's standard mapping tables, or by his two-term continued fraction for the parameter partials. The definition of Eq. (20) lends itself to easy computation of $\rho_{Z_{\text{dry}}}$ and $\rho_{Z_{\text{wet}}}$ as adjustment parameters if the user wishes to "tune" these parameters in the data filtering or estimation process. Hence,

$$\frac{\partial\rho_{\text{trop}}(E)}{\partial\rho_{Z_{\text{dry}}}} \equiv R_{\text{dry}}(E) \tag{21}$$

and

$$\frac{\partial\rho_{\text{trop}}(E)}{\partial\rho_{Z_{\text{wet}}}} \equiv R_{\text{wet}}(E) \tag{22}$$

Since the mapping factors, $R_{\text{dry}}(E)$ and $R_{\text{wet}}(E)$, are functions of the incident elevation angle of the signal path, they can be computed by numerical ray tracing methods or can be approximated analytically. Ray tracing offers greater accuracy, particularly in the low elevation angle regimes where the tropospheric effect is difficult to model, but is often time consuming and impractical under varying atmospheric conditions. Often what is done in practice is to derive "fitted" empirically based formulas from numerical ray traces of either an idealized refractivity profile or from actual radiosonde profile data. Another less traditional approach is to derive an analytic approximation of the tropospheric mapping based on an idealized refractivity profile.

Marini [1972] showed that the tropospheric mapping could be very accurately modeled by a continued fraction expansion of the form

$$R(E) = \cfrac{1}{\sin E + \cfrac{a}{\sin E + \cfrac{b}{\sin E + \cfrac{c}{\sin E + \cdots}}}} \tag{23}$$

where the constants, a, b, c, ... , give the elevation dependence of the tropospheric delay. The more terms carried out in the expansion, the better the approximation of the geometrical bending effect. Indeed, most of the candidate mapping functions presented in this section are based on this formula, with the empirical constants parameterized for surface meteorological measurements. Consequently, these "improved" mapping functions can be adapted to a wide variety of applications under varying weather conditions.

Recall that in Chao's two-term continued fraction model [*cf.*, Eq. (7)], the normalization factor, tan E, was used in order to ensure a mapping factor of unity at zenith. This is consistent with the simple definition given by Eq. (20). The mapping function of Eq. (23), however, does not ensure this property. Therefore, a "normalized" form of the Marini mapping function is often used instead, which takes the form

$$R(E) = \frac{1 + a/(1 + b/(1 + c/(1 + \cdots)))}{\sin E + \cfrac{a}{\sin E + \cfrac{b}{\sin E + \cfrac{c}{\sin E + \cdots}}}} \tag{24}$$

This normalization process is preferred over the use of tan E since the latter can introduce a bias in the mapping function due its slower convergence property over a direct sin E calculation [*Davis et al.*, 1985]. In addition, a direct sin E calculation is not subject to an inherent analytic singularity at zenith (as is tan E).

In this section, five highly accurate tropospheric mapping models are presented which are considered to be the "state of the art." Of the five candidate models described herein, only one, the Lanyi mapping function [*Lanyi*, 1983; 1984], does not explicitly separate the dry and wet components, but rather combines them into a single mapping function based on an analytic expansion of the tropospheric delay in terms of moments of the dry and wet refractivity. The remaining candidate models were empirically derived and include the "CfA-2.2" of *Davis et al.* [1985], the Ifadis global solution model [*Ifadis*, 1986], the "MTT" functions of Herring [*Herring*, 1992], and the "NMF" functions of Niell [*Niell*, 1993; 1994a; 1994b]. It is important to note that all of the mapping functions presented in this report (both current and proposed) were derived under the assumption of a spherically symmetric atmosphere, *i.e.*, none of the mapping functions implicitly or explicitly account for the effects of azimuthal asymmetry.

4.1 Lanyi Mapping Function

In analyses of intercontinental VLBI data, it was found that the Chao semi-empirical mapping function was inadequate for high-precision experiments. In 1983, G. E. Lanyi presented an analytic tropospheric mapping function which was found to be more accurate than Chao's tables and analytic approximations, as well as a variety of other earlier mapping functions, above 4° elevation [*Lanyi*, 1983]. These results were published later in an external

report [*Lanyi*, 1984]. Although there have been many atmospheric modeling improvements in recent years, Lanyi's method arguably appears to be the most robust and complete model of its kind, adaptable to a wide variety of experiments involving radio interferometry and GPS-based analysis [*McCarthy*, 1992]. Its principal advantage is that the mathematical expansion used in the derivation is valid for any laterally homogenous atmospheric model of refractivity. Lanyi's analytic approximation is estimated to be in error (*i.e.*, differ from ray trace calculations) by less than 0.02% for elevation angles larger than 6°, less than 4 mm at 6°, and approximately 0.004% or 0.3 mm at 20° [*Lanyi*, 1984].

In its simplest form, in which no meteorological information is available, the Lanyi mapping function employs standard, or "average," values of atmospheric model parameters. Provision is made for specifying surface meteorological data acquired at the time of observation, that may override the nominal values of the model parameters. The dry and wet components of the tropospheric mapping are not in the Lanyi model but rather combined into a single nonlinear mapping function by expanding the dry, wet, and bending contributions to the atmospheric delay in terms of moments of refractivity. The following compact mathematical description of the Lanyi mapping function has been adapted from *Sovers and Jacobs* [1994] but is repeated and expanded here for completeness.

The Lanyi one-way range tropospheric correction is defined by

$$\Delta\rho_{\text{Lanyi}}(E) \equiv F(E) / \sin E \tag{25}$$

where

$$\begin{aligned} F(E) = {} & \rho_{Z_{\text{dry}}} F_{\text{dry}}(E) + \rho_{Z_{\text{wet}}} F_{\text{wet}}(E) \\ & + \left[\rho^2_{Z_{\text{dry}}} F_{\text{bend1}}(E) + 2\rho_{Z_{\text{dry}}}\rho_{Z_{\text{wet}}} F_{\text{bend2}}(E) + \rho^2_{Z_{\text{wet}}} F_{\text{bend3}}(E)\right] / \Delta \\ & + \rho^3_{Z_{\text{dry}}} F_{\text{bend4}}(E) / \Delta^2 \end{aligned} \tag{26}$$

The quantities $\rho_{Z_{\text{dry}}}$ and $\rho_{Z_{\text{wet}}}$ are the usual zenith dry and wet tropospheric delays; Δ is the atmospheric scale height given by $\Delta = kT_0/mg_c$, with k the Boltzmann's constant in erg/K, T_0 the average surface temperature in kelvin, m the mean molecular mass of dry air in grams, and g_c the gravitational acceleration at the center of gravity of the air column in erg/g•cm. Using the standard values $k = 1.38066 \times 10^{-16}$ erg/K, $m = 4.8097 \times 10^{-23}$ g, $g_c = 978.37$ erg/g•cm, and the average temperature for DSN stations $T_0 = 292$ K, the atmospheric scale height is computed to be $\Delta = 8567$ m.

The dry, wet, and bending terms are expressed as of moments of the refractivity:

$$F_{\text{dry}}(E) = A_{10}(E) G\left(\lambda M_{110}, u\right) + 3\sigma u M_{210} G^3\left(M_{110}, u\right) / 2 \tag{27a}$$

$$F_{\text{wet}}(E) = A_{01}(E) G\left(\lambda M_{101}/M_{001}, u\right) / M_{001} \tag{27b}$$

$$F_{\text{bend1}}(E) = \left[\sigma G^3(M_{110}, u)/\sin^2 E - M_{020} G^3(M_{120}/M_{020}, u)\right] / 2\tan^2 E \quad (27c)$$

$$F_{\text{bend2}}(E) = -M_{011} G^3(M_{111}/M_{011}, u) / 2 M_{001} \tan^2 E \quad (27d)$$

$$F_{\text{bend3}}(E) = -M_{002} G^3(M_{102}/M_{002}, u) / 2 M_{001}^2 \tan^2 E \quad (27e)$$

$$F_{\text{bend4}}(E) = M_{030} G^3(M_{130}/M_{030}, u) / \tan^4 E \quad (27f)$$

Note that in *Lanyi* [1984], there are two misprints in the corresponding equations. In Eq. (3) of the referenced document, the misprinted factor of 3/4 should be replaced by 3/2, while in Eq. (5) of the referenced document, the erroneous multiplier of -1/2 in the $F_{\text{bend4}}(E)$ term should be removed [*Lanyi*, 1993]. These changes are reflected in the above equations. $G(q,u)$ is a geometric factor given by

$$G(q,u) = (1 + qu)^{-1/2} \quad (28)$$

with

$$u = 2\sigma / \tan^2 E \quad (29)$$

where $\sigma = \Delta/R$ is a measure of the curvature of the Earth's surface with standard value 0.001345. An approximation for the local radius of curvature, R, is given in Eq. (37) below.

The quantities $A_{lm}(E)$ and M_{ilm} are related to moments of the atmospheric refractivity. $A_{10}(E)$ involves the dry refractivity, while $A_{01}(E)$ is the corresponding wet quantity. The $A_{lm}(E)$ are given by

$$A_{lm}(E) = M_{0lm} + \sum_{n=1}^{10} \sum_{k=0}^{n} \frac{(-1)^{n+k}(2n-1)!!M_{n-k,l,m}}{2^n k!(n-k)!} \left[\frac{u}{1 + \lambda u M_{1lm}/M_{0lm}}\right]^n \left[\frac{\lambda M_{1lm}}{M_{0lm}}\right]^k \quad (30)$$

with the scale factor $\lambda = 3$ for $E < 10°$ and $\lambda = 1$ for $E > 10°$. Only the two combinations $(l,m) = (0,1)$ and $(1,0)$ are needed for the $A_{lm}(E)$. The moments of the dry and wet refractivities are defined as

$$M_{nij} \equiv \int_0^\infty dq\, q^n f_{\text{dry}}^i(q) f_{\text{wet}}^j(q) \quad (31)$$

where $f_{\text{dry,wet}}(q)$ are the surface-normalized refractivities. Here, n ranges from 0 to 10, i from 0 to 3, and j from 0 to 2; not all combinations are needed. Carrying out the integration in Eq. (31) for a three-section temperature profile gives an expression for the general moment, M_{nij}:

$$M_{nij}/n! = (1 - e^{-aq_1})/a^{n+1} + e^{-aq_1}\left[1 - T_2^{b+n+1}(q_1,q_2)\right]\prod_{i=0}^{n}\frac{a}{b+i+1}$$
$$+ e^{-aq_1}T_2^{b+n+1}(q_1,q_2)/a^{n+1} \qquad (32)$$

Here,

$$T_2(q_1,q_2) = 1 - (q_2 - q_1)/\alpha \qquad (33)$$

The quantities q_1 and q_2 are the scale-height normalized inversion and tropopause altitudes, respectively. For the standard atmospheric model, $q_1 = 0.1459$ and $q_2 = 1.424$. The constants a and b are functions of the dry ($\alpha = 5.0$) and wet ($\beta = 3.5$) model parameters, as well as of the powers of the refractivities (i and j) in the moment definitions. Table 3 gives the necessary a's and b's for the current mechanization (version "42map" 30-sep-85). Note that the normalization is such that $M_{010} = 1$; this moment has therefore been excluded from Eqs. (27a) through (27f).

Table 3. Dependence of constants *a* and *b* on the Lanyi tropospheric model parameters α and β (version "42map" 30-Sep-85).

i	j	Moment Type	a	b
1	0	dry	1	$\alpha - 1$
0	1	wet	β	$\alpha\beta - 2$
2	0	dry squared	2	$2(\alpha - 1)$
1	1	dry times wet	$\beta + 1$	$\beta(\alpha+1) - 3$
0	2	wet squared	2β	$2(\alpha\beta - 2)$
3	0	dry cubed	3	$3(\alpha - 1)$

Provision is made for input of four meteorological parameters to override the nominal (average) values of the Lanyi model. These are: 1) the surface temperature, T_0, which determines the atmospheric scale height (nominal value 292 K); 2) the temperature lapse rate, w, which determines the dry model parameter α (nominal values $w = -6.8165$ K/km, $\alpha = 5.0$); 3) the inversion altitude, h_1, which determines $q_1 = h_1/\Delta$ (nominal value $h_1 = 1.25$ km); and 4) the tropopause altitude, h_2, which determines $q_2 = h_2/\Delta$ (nominal value $h_2 = 12.2$ km). A fifth parameter, the surface pressure, P_0, is not currently used. Approximate sensitivity of the tropospheric delay (at 6° elevation) to the meteorological parameters is -0.7 cm/K for surface temperature, -2 cm/(K/km) for lapse rate, and -2 cm/km for inversion and 0.5 cm/km for tropopause altitudes, respectively.

In addition, there are two site-dependent parameters which may be input to override the standard values. The first is the gravitational acceleration at the center of gravity of the air column, g_c, defined earlier with a nominal value of 978.37 erg/g•cm. Recall that it is used, along

with surface temperature, T_0, to determine the atmospheric scale height Δ. The gravity term, g_c, can be approximated as [*Lanyi*, 1983]:

$$g_c \approx g_0 - 2(kT_0/mR)M_{010} \tag{34}$$

The second term in the difference represents the "shift" in gravity (~2.25 erg/g•cm), which is a function of surface temperature and temperature profile parameters. The approximate surface value of g (erg/g•cm) comes from *Saastamoinen* [1972]:

$$g_0 \approx 980.62\,(1 - 0.00265 \cos 2\varphi - 0.00031\,H_c) \tag{35}$$

where φ is the geodetic latitude of the station in degrees, and H_c is the height in kilometers of the center of mass of the vertical column of air. The default value for g_0 is taken to be 980.62 erg/g•cm, corresponding to gravitational acceleration at sea level ($H_c = 0$) and midlatitude ($\varphi = 45°$). Because of the difficulty in implementing Eq. (34), Saastamoinen's "average" approximation formula is often used for computing the site-dependent variability of gravity [*cf.*, Eq. (13)]:

$$g_c = 978.4\,(1 - 0.00266 \cos 2\varphi - 0.00028\,H_s) \tag{36}$$

where H_s is the MSL height of the station in kilometers.

The other site-dependent quantity, which is used to determine the variation of g_0 as well as the Earth curvature parameter, σ, is the local radius of curvature, R, which can be approximated as

$$R \approx R_e\,(1 - 0.003353 \cos 2\varphi + 0.000157\,H_s) \tag{37}$$

Here, R_e is the mean equatorial radius of Earth (default value 6378.16 km).

In analysis of data for which meteorological parameters are not available, there is an approximate form of the mapping function (again, version "42map") which involves a one-parameter estimate. This parameter, simply denoted here as p, accounts for deviations from standard meteorological conditions. It is a modified form of the ~$1/\tan^2 E$ term but includes wet *a priori* shift values and is more realistic at low elevation angles than $1/\tan^2 E$. The bending effect is not included in this approximation, as it is assumed to be modeled sufficiently by solving for the zenith dry plus wet delay, hence, the dry and wet atmospheric refractivity factors $A_{10}(E)$ and $A_{01}(E)$ are taken to be unity. For this special case, the one-parameter correction is a fraction of the approximate tropospheric correction to $(\rho_{Z_{dry}} + \rho_{Z_{wet}}) / \sin E$:

$$\Delta\rho_{\text{Lanyi}}(E) \equiv (\rho_{Z_{dry}} + \rho_{Z_{wet}}) / \sin E + p\,\frac{\partial \Delta\rho_{\text{Lanyi}}(E)}{\partial p} \tag{38}$$

The partial derivative term is given by

$$\frac{\partial \Delta\rho_{\text{Lanyi}}(E)}{\partial p} = -\frac{(\rho_{Z_{\text{dry}}} + \rho_{Z_{\text{wet}}})uM_{110}}{G(M_{110}, u)[1 + G(M_{110}, u)]\sin E} + \frac{\rho_{Z_{\text{wet}}}u(M_{110} - M_{101}/M_{001})}{G(M_{110}, u)G(M_{101}/M_{001}, u)[G(M_{110}, u) + G(M_{101}/M_{001}, u)]\sin E} \tag{39}$$

Because the definition of the one-way range tropospheric correction for the Lanyi model does not explicitly separate the dry and wet components, as in Eq. (20), the parameter partials for the conventional tuning parameters, $\rho_{Z_{\text{dry}}}$ and $\rho_{Z_{\text{wet}}}$, are expressed as

$$\frac{\partial \Delta\rho_{\text{Lanyi}}(E)}{\partial \rho_{Z_{\text{dry}}}} = \left[F_{\text{dry}}(E) + 2\rho_{Z_{\text{dry}}}F_{\text{bend1}}(E) / \Delta\right] / \sin E + \left[2\rho_{Z_{\text{wet}}}F_{\text{bend2}}(E) / \Delta + 3\rho_{Z_{\text{dry}}}^2 F_{\text{bend4}}(E) / \Delta^2\right] / \sin E \tag{40}$$

$$\frac{\partial \Delta\rho_{\text{Lanyi}}(E)}{\partial \rho_{Z_{\text{wet}}}} = \left[F_{\text{wet}}(E) + 2\rho_{Z_{\text{dry}}}F_{\text{bend2}}(E) / \Delta + 2\rho_{Z_{\text{wet}}}F_{\text{bend3}}(E) / \Delta\right] / \sin E \tag{41}$$

4.2 Davis et al. ("CfA-2.2") Mapping Function

Around the same time that Lanyi published his new mapping function, scientists from the U.S. East Coast VLBI community were developing a new empirically based formula for the dry component of the tropospheric mapping. The resulting mapping function, designated "CfA-2.2," was introduced by J. L. Davis and his colleagues in 1985 and resulted from extending Chao's empirical formula in the form of a three-term Marini continued fraction, fit to ray traces of an idealized atmospheric model of refractivity [*Davis et al.*, 1985]. Additionally, the mapping function was parameterized for surface meteorological measurements; namely, surface pressure and temperature, relative humidity, lapse rate, and tropopause altitude. A companion mapping function for the wet component of the delay was not derived. The CfA-2.2 mapping function is estimated to deviate from ray trace calculations by less than 5 mm for elevation angles down to 5° [*Davis et al.*, 1985].

The mapping function, denoted here as $R_{\text{CfA-2.2}}(E)$, is given by

$$R_{\text{CfA-2.2}}(E) = \frac{1}{\sin E + \dfrac{a}{\tan E + \dfrac{b}{\sin E + c}}} \tag{42}$$

where the three parameters a, b, and c are expressed in terms of meteorological data as:

$$a = 0.001185\left[1 + 0.6071 \times 10^{-4}(P_0 - 1000) - 0.1471 \times 10^{-3}e_0 + 0.3072 \times 10^{-2}(T_0 - 293.15) + 0.1965 \times 10^{-1}(w + 6.5) - 0.5645 \times 10^{-2}(h_2 - 11.231)\right] \quad (43a)$$

$$b = 0.001144\left[1 + 0.1164 \times 10^{-4}(P_0 - 1000) + 0.2795 \times 10^{-3}e_0 + 0.3109 \times 10^{-2}(T_0 - 293.15) + 0.3038 \times 10^{-1}(w + 6.5) - 0.1217 \times 10^{-1}(h_2 - 11.231)\right] \quad (43b)$$

$$c = -0.0090 \quad (43c)$$

Here, P_0 is the total surface pressure measured in millibars, and e_0 is the partial pressure of water vapor at the surface, also measured in millibars. Nominal values are taken to be $P_0 = 1000$ mbar and $e_0 = 0$. T_0 is the surface temperature, originally given in degrees Celsius but shown here in kelvin for consistency with the Lanyi mapping function, w is the temperature lapse rate (by definition, $w < 0$) in K/km, and h_2 is the altitude of the tropopause in kilometers. The nominal values for these parameters are $T_0 = 293.15$ K (= 20 °C), w = -6.5 K/km, and $h_2 = 11.231$ km. Approximate sensitivity of the tropospheric delay (at 5° elevation) to the meteorological parameters is [*Davis et al.*, 1985]: -0.17 cm/mbar for surface pressure, -0.75 cm/K for surface temperature, -4.4 cm/(K/km) for lapse rate, and 1.1 cm/km for tropopause altitude.

When evaluating the performance of this new mapping function with VLBI data for a multistation intercontinental geodetic experiment, Davis et al. used the CfA-2.2 to represent both the dry and wet mapping components of the delay. By not using a mapping function derived explicitly for the wet component, a small error was introduced in the VLBI results, as the wet zenith correction was multiplied by the difference between the CfA-2.2 and the "true" wet mapping function [*Davis et al.*, 1985]. An alternative approach sometimes used in practice is to utilize the CfA-2.2 mapping function for the dry component of the delay and the Chao wet mapping function for the wet component (see *e.g.*, *MacMillan and Ma* [1994]).

4.3 Ifadis Global Mapping Functions

An extensive study of newly proposed global-, site-, and climate-dependent tropospheric calibration models was conducted by I. I. Ifadis and published in 1986 [*Ifadis*, 1986]. Ifadis' new models for the zenith delay calibration and tropospheric mapping were based on ray trace analyses of radiosonde profiles collected from various sites distributed over large areas of the world and under different climactic conditions. More specifically, the data base used in his study consisted of height profiles of pressure, temperature, and relative humidity, as well as wind speed and direction, which were collected over a 3 year period from 47 globally distributed sites.

Ifadis derived dry and wet mapping functions based on the "unnormalized" continued fraction form of Marini [Eq. (23)], truncated at three terms and at four terms in the expansion. Different mapping coefficients were derived depending on whether the global-, site-, or climate-dependent model was being used, but all are linear functions of surface temperature, pressure, and relative humidity. Because a great deal of care has to be exercised when using the climate-dependent model or in "optimizing" the mapping coefficients for the site-dependent model, only the global-solution model is referred to in this report. The Ifadis three-term global mapping function is estimated to be in error by less than 4 mm at 2° elevation [*Ifadis*, 1986].

In order to be consistent with the definition of Eq. (20), a normalized form of the Ifadis global mapping function is assumed herein, which takes the form

$$R_{\text{Ifadis},i}(E) = \cfrac{1 + a_i / (1 + b_i/(1 + c_i))}{\sin E + \cfrac{a_i}{\sin E + \cfrac{b_i}{\sin E + c_i}}} \tag{44}$$

where, for i = dry:

$$a_{\text{dry}} = 0.001237 + 0.1316 \times 10^{-6}(P_0 - 1000) + 0.1378 \times 10^{-5}(T_0 - 288.15) + 0.8057 \times 10^{-5}\sqrt{e_0} \tag{45a}$$

$$b_{\text{dry}} = 0.003333 + 0.1946 \times 10^{-6}(P_0 - 1000) + 0.1040 \times 10^{-5}(T_0 - 288.15) + 0.1747 \times 10^{-4}\sqrt{e_0} \tag{45b}$$

$$c_{\text{dry}} = 0.078 \tag{45c}$$

and, for i = wet:

$$a_{\text{wet}} = 0.0005236 + 0.2471 \times 10^{-6}(P_0 - 1000) - 0.1724 \times 10^{-6}(T_0 - 288.15) + 0.1328 \times 10^{-4}\sqrt{e_0} \tag{46a}$$

$$b_{\text{wet}} = 0.001705 + 0.7384 \times 10^{-6}(P_0 - 1000) + 0.3767 \times 10^{-6}(T_0 - 288.15) + 0.2147 \times 10^{-4}\sqrt{e_0} \tag{46b}$$

$$c_{\text{wet}} = 0.05917 \tag{46c}$$

A misprint in Eq. (6.10b) of Ifadis' original report for the b_{dry} coefficient has been corrected here [*MacMillan*, 1994]. The meteorological parameters used in the mapping coefficients are defined as P_0 for surface pressure in millibars, T_0 for surface temperature (shown here in kelvin) and e_0 for the partial pressure of water vapor in millibars. Nominal values for these parameters are $P_0 = 1000$ mbar, $T_0 = 288.15$ K (= 15 °C), and $e_0 = 0$.

4.4 Herring ("MTT") Mapping Functions

The "MTT" dry and wet mapping functions were introduced by T. A. Herring (co-author of the CfA-2.2 dry mapping function) in 1992 [*Herring*, 1992]. The MTT mapping functions provide empirically based formulas for both the dry and wet components of the tropospheric effect and take the form of three-term normalized Marini continued fractions. The coefficients of the mapping function are linear functions of surface temperature (which is the only parameterized meteorological input) and station geodetic latitude and height. The dry and wet mapping functions were fit to ray traces of 2 years of atmospheric profiles from 11 North American sites. The MTT mapping function is estimated to be in error by less than 1 mm at 5° elevation, if the coefficients in the mapping function are known, and ~30 mm if the coefficients are determined from their correlation with location and surface temperature [*Herring*, 1992].

The function corresponding to the dry and wet mapping is given by

$$R_{MTT_i}(E) = \frac{1 + a_i / (1 + b_i/(1 + c_i))}{\sin E + \dfrac{a_i}{\sin E + \dfrac{b_i}{\sin E + c_i}}} \tag{47}$$

where, for i = dry:

$$a_{dry} = \left[1.2320 + 0.0139 \cos \varphi - 0.0209 H_s + 0.00215 (T_0 - 283.15)\right] \cdot 10^{-3} \tag{48a}$$

$$b_{dry} = \left[3.1612 - 0.1600 \cos \varphi - 0.0331 H_s + 0.00206 (T_0 - 283.15)\right] \cdot 10^{-3} \tag{48b}$$

$$c_{dry} = \left[71.244 - 4.293 \cos \varphi - 0.149 H_s - 0.0021 (T_0 - 283.15)\right] \cdot 10^{-3} \tag{48c}$$

and, for i = wet:

$$a_{wet} = \left[0.583 - 0.011 \cos \varphi - 0.052 H_s + 0.0014 (T_0 - 283.15)\right] \cdot 10^{-3} \tag{49a}$$

$$b_{wet} = \left[1.402 - 0.102 \cos \varphi - 0.101 H_s + 0.0020 (T_0 - 283.15)\right] \cdot 10^{-3} \tag{49b}$$

$$c_{wet} = \left[45.85 - 1.91 \cos \varphi - 1.29 H_s + 0.015 (T_0 - 283.15)\right] \cdot 10^{-3} \tag{49c}$$

Here, φ and H_s denote the geodetic latitude and MSL height of the station, respectively, with φ specified in degrees and H_s in kilometers; T_0 is the surface temperature (again, shown in kelvin) with nominal value $T_0 = 283.15$ K (= 10 °C).

4.5 Niell ("NMF") Mapping Functions

All of the candidate mapping functions discussed thus far have either been based on parameterizations of surface meteorology or have some direct dependence on surface meteorological data. A somewhat different approach was suggested recently by A. E. Niell [*Niell*, 1993; 1994a; 1994b]. Niell claims that mapping functions which depend on surface temperature are limited in their accuracy since the variability in temperature near the Earth's surface is much greater than at higher (> 2000 m) altitudes. Therefore, he based his mapping functions (dry and wet) on temporal fluctuations in the bulk of the atmosphere rather than on meteorological conditions near the surface. The Niell global mapping functions, designated "NMF," were derived from temperature and relative humidity profiles of the U.S. Standard Atmosphere at North latitude regions 15° (tropical), 30° (subtropical), 45° (midlatitude), 60° (subarctic), and 75° (subarctic) for the months of January (Winter) and July (Summer). Niell assumes that the Southern and Northern hemispheres are anti-symmetric in time, *i.e.*, that the seasonal behavior is the same. In addition, he assumes that the equatorial region is described by the 15° N latitude profile while the polar regions are described by the 75° N latitude profile. The NMF mapping functions are estimated to be in error by less than 4 mm from 12° down to 3°, comparable to the MTT mapping functions of Herring, but with smaller biases relative to ray traces than the MTT functions [*Niell*, 1994a].

The NMF mapping functions utilize the same normalized continued fraction expansion of Marini that was used in the Ifadis and MTT dry and wet mapping functions, truncated at three terms, but with considerably different parameterizations of the mapping coefficients. In addition, the NMF dry mapping function contains a correction term to account for a geoidal station height dependence, reflecting the fact that the ratio of the atmosphere "thickness" to the radius of curvature decreases with height [*Niell*, 1994b].

The NMF dry mapping function can be expressed as

$$R_{\mathrm{NMF_{dry}}}(E) = m_{\mathrm{dry}}(E) + \Delta m_{\mathrm{dry}}(E) \tag{50}$$

where

$$m_{\mathrm{dry}}(E) = \frac{1 + a_{\mathrm{dry}}/(1 + b_{\mathrm{dry}}/(1 + c_{\mathrm{dry}}))}{\sin E + \dfrac{a_{\mathrm{dry}}}{\sin E + \dfrac{b_{\mathrm{dry}}}{\sin E + c_{\mathrm{dry}}}}} \tag{51}$$

The mapping coefficients, a_{dry}, b_{dry}, and c_{dry}, are linear functions of tabular latitude φ_i, at time t from January 0.0 (in UT days):

$$a_{dry}(\varphi_i,t) = a_{dry_{avg}}(\varphi_i) + a_{dry_{amp}}(\varphi_i)\cos\left[\frac{t - T_0}{365.25}\right] \quad (52)$$

Similar equations exist for the b_{dry} and c_{dry} mapping coefficients. Here, T_0 denotes the "phase" in UT days past January 0.0 and not the surface temperature as in earlier mapping function descriptions. A nominal value of T_0 = 28 days is used in the current version of the dry (hydrostatic) mapping function (designated "nmfh2" 26-Jan-94), corresponding to the day that exhibited the maximum value of the mapping function based on data analysis. The latitude dependence reflects the five different latitude regions discussed earlier (at 15°, 30°, 45°, 60°, and 75° N), thus, i ranges from 1 to 5 in Eq. (52). The average (avg) and amplitude (amp) coefficients are given in Table 4a. Intermediate values for the mapping coefficients are obtained by linear interpolation.

Table 4a. Mapping function coefficients for the dry (hydrostatic) NMF mapping function (version "nmfh2" 26-Jan-94).

Coefficient	Latitude				
	15°	30°	45°	60°	75°
			average ($\times 10^{-3}$)		
$a_{dry_{avg}}$	1.2769934	1.2683230	1.2465397	1.2196049	1.2045996
$b_{dry_{avg}}$	2.9153695	2.9152299	2.9288445	2.9022565	2.9024912
$c_{dry_{avg}}$	62.610505	62.837393	63.721774	63.824265	64.258455
			amplitude ($\times 10^{-5}$)		
$a_{dry_{amp}}$	0.0	1.2709626	2.6523662	3.4000452	4.1202191
$b_{dry_{amp}}$	0.0	2.1414979	3.0160779	7.2562722	11.723375
$c_{dry_{amp}}$	0.0	9.0128400	4.3497037	84.795348	170.37206

The correction term, $\Delta m_{dry}(E)$, is given by

$$\Delta m_{dry}(E) = \frac{dm_{dry}(E)}{dh} H_s \quad (53)$$

where H_S is the MSL height of the station. The analytic height correction coefficient, $dm_{dry}(E) / dh$, is taken to be

$$\frac{dm_{dry}(E)}{dh} = \frac{1}{\sin E} - f(E;a_{ht},b_{ht},c_{ht}) \quad (54)$$

Here, $f(E;a_{ht},b_{ht},c_{ht})$ represents the three-term continued fraction expressed by Eq. (51) using the following values for the "fitted" height parameters:

$$a_{ht} = 2.53 \times 10^{-5} \tag{55a}$$

$$b_{ht} = 5.49 \times 10^{-3} \tag{55b}$$

$$c_{ht} = 1.14 \times 10^{-3} \tag{55c}$$

Because only the latitude dependence is predictable for the corresponding wet mapping function, it takes a simpler form:

$$R_{\mathrm{NMF_{wet}}}(E) = \cfrac{1 + a_{\mathrm{wet}}/(1 + b_{\mathrm{wet}}/(1 + c_{\mathrm{wet}}))}{\sin E + \cfrac{a_{\mathrm{wet}}}{\sin E + \cfrac{b_{\mathrm{wet}}}{\sin E + c_{\mathrm{wet}}}}} \tag{56}$$

The values for the a_{wet}, b_{wet}, and c_{wet} coefficients are provided in Table 4b, corresponding to the five different latitude regions. As with the dry mapping coefficients, intermediate values not shown in the table are determined by linear interpolation. The current version of the wet mapping function is designated "nmfw2."

Table 4b. Mapping function coefficients for the wet NMF mapping function (version "nmfw2" 26-Jan-94).

Coefficient	Latitude				
	15°	30°	45°	60°	75°
			($\times 10^{-4}$)		
a_{wet}	5.8021897	5.6794847	5.8118019	5.9727542	6.1641693
			($\times 10^{-3}$)		
b_{wet}	1.4275268	1.5138625	1.4572752	1.5007428	1.7599082
			($\times 10^{-2}$)		
c_{wet}	4.3472961	4.6729510	4.3908931	4.4626982	5.4736038

SECTION 5

EXPERIMENTAL EVALUATION

Because ray tracing through an extensive radiosonde data set was recently conducted [see *Mendes and Langley*, 1994], no attempt was made here to perform additional ray tracing computations to evaluate the performance of the candidate tropospheric mapping functions presented thus far. The Mendes-Langley study culminated in a comprehensive analysis covering different climatic regions of a number of tropospheric mapping functions currently used in academia and industry, including all of the mapping functions described in this report. In an effort to be complete, this section describes a recent statistical evaluation of the candidate tropospheric mapping functions based on actual VLBI data acquired by the DSN.

5.1 Overview

Tests were devised to evaluate the performance of various tropospheric mapping functions using VLBI measurements with DSN antennas carried out during the past 2 decades [*Sovers and Lanyi*, 1994]. These are typically 24-hour observing sessions using two antennas separated by either of the two intercontinental baselines (~8,400 or 10,600 km), looking over as large a region of the sky as permitted by mutual source visibility. Because the extreme baseline length is a large fraction of an Earth diameter, the region of the sky accessible at either site is severely limited, and numerous observations are made at the lower elevation limits of the antennas (~6°). These low-elevation observations help to decorrelate zenith delays at the two stations in data analyses, but require high accuracy in the tropospheric mapping at low elevation angles. While tropospheric delay is also an important part of the theoretical model in orbit determination with the ODP software set [*Mottinger*, 1982], similar tests for the Doppler and range observables in spacecraft tracking are precluded by the lack of accepted observations below 15° elevation, which is the region most sensitive to details of the mapping algorithms.

In order to avoid the possibility of drawing false conclusions induced by the much higher system noise level of the early observations (Mark II ~10 cm, Mark III ~2 cm), only a subset of the VLBI data was selected for detailed analyses. It included all the newer data, and was recorded with Mark III data acquisition systems. The data spanned the time period 1988 to 1993; a total of 11,897 delay and delay rate pairs were used. A standard VLBI parameter estimation fit was performed using JPL's MODel ESTimation (MODEST) software set [*Sovers and Jacobs*, 1994]. The estimated parameters included positional coordinates of 283 radio sources, a pair of nutation angle offsets for each session (longitude and obliquity), and station coordinates for each overseas station (Australia and Spain) for each of the 61 sessions. The right ascension of one source, the nutation model on one day, and the Goldstone station coordinates were kept fixed. A new value of the zenith tropospheric value was estimated every 2 hours at each station. Correlations among the delay and delay rate observables due to tropospheric fluctuations were ignored here, but will be considered in a future study. More details of both the DSN data acquisition and parameter estimation procedures have been previously published [*Sovers et al.*,

1988; *Sovers*, 1991]. *MacMillan and Ma* [1994] recently performed a similar evaluation for the Chao, CfA-2.2, Ifadis, and MTT tropospheric mapping functions, using the NASA Crustal Dynamics and IRIS databases.

A post-fit analysis estimates linear time variation of the station coordinates, as well as the Goldstone–overseas baseline lengths. Such fits and post-fit baseline analyses were repeated for each of ten tropospheric mapping functions, with all other aspects of modeling and parameter estimation (the latter with one exception) being identical. The mapping functions are listed in Table 5. For those functions requiring surface meteorological measurements (No.s 4 through 9) data were taken from the DSCC Media Calibration Subsystem database [*Runge*, 1993]. Temperature lapse rates had seasonal variations at the Australia and Spain stations [*Smith*, 1992], while the default w = -6.8165 K/km was used for Goldstone. The two remaining atmospheric parameters (inversion and tropopause heights) were assigned default values of h_1 = 1.25 and h_2 = 12.2 km, respectively. The "Lanyi estimated" function requires some additional explanation. It uses the *Lanyi* [1984] function to accurately map the zenith delays, based on the available tabulated surface and balloon meteorological data. A crude single-parameter approximation is then used to account for the effect of deviations between the real and tabulated meteorological data on the mapping function [*cf.*, Section 4.1]. One such parameter is estimated at each station for every observing session.

Table 5. Tropospheric mapping functions used in fits to DSN VLBI data.

Mapping Function	JPL VLBI Archive ID	Reference	Comments
1 = Chao original	152	[*Chao*, 1974]	
2 = Chao revised	153	—	Revised constants
3 = Chao tables	154	[*Chao*, 1977]	Tables used in ODP
4 = Lanyi standard	151	[*Lanyi*, 1984]	
5 = Lanyi updated	155	[*Lanyi*, 1983]	Geometry and gravity curvature corrections
6 = Lanyi estimated	156	[*Sovers and Jacobs*, 1994]	One parameter/station estim. per 24-h expt.
7 = CfA-2.2	158	[*Davis et al.*, 1985]	
8 = Ifadis	157	[*Ifadis*, 1986]	
9 = MTT	159	[*Herring*, 1992]	
10 = NMF	160	[*Niell*, 1993; 1994a; 1994b]	

Examination of tropospheric mapping functions includes: 1) comparison of the functional forms of the various mapping functions for the DSN sites for the particular subset of meteorological conditions prevailing at the times of the VLBI measurements, and 2) comparison of VLBI delay and delay rate residuals and baseline length scatter resulting from multi-parameter estimation in model fits to the VLBI observables. The first category thus reflects the effect on the mapping functions of the elevation distributions and weather conditions at the times of VLBI

experiments, while the second category is a quantitative assessment of how well each mapping function represented the data. These two categories of tests are described in greater detail below.

5.2 Statistics of Mapping Function Delay Values

Direct comparisons yield voluminous data, most of which will not be presented here. They are in essential agreement with the results presented by *Mendes and Langley* [1994]. Discrepancies between mapping functions generally increase rapidly with decreasing elevation angle, in most cases reaching ~10 cm of tropospheric delay at the DSN lower observational limit of 6°. A histogram of the elevation angles of the DSN VLBI observations is shown in Figure 5. The distribution is seen to peak between 10° and 15°, with more than half of the observations being below 30° elevation at one or both ends of the baseline. This distribution of observations with elevation angle, along with the magnitude of the differences between the mapping functions, is generally consistent with the post-fit analyses.

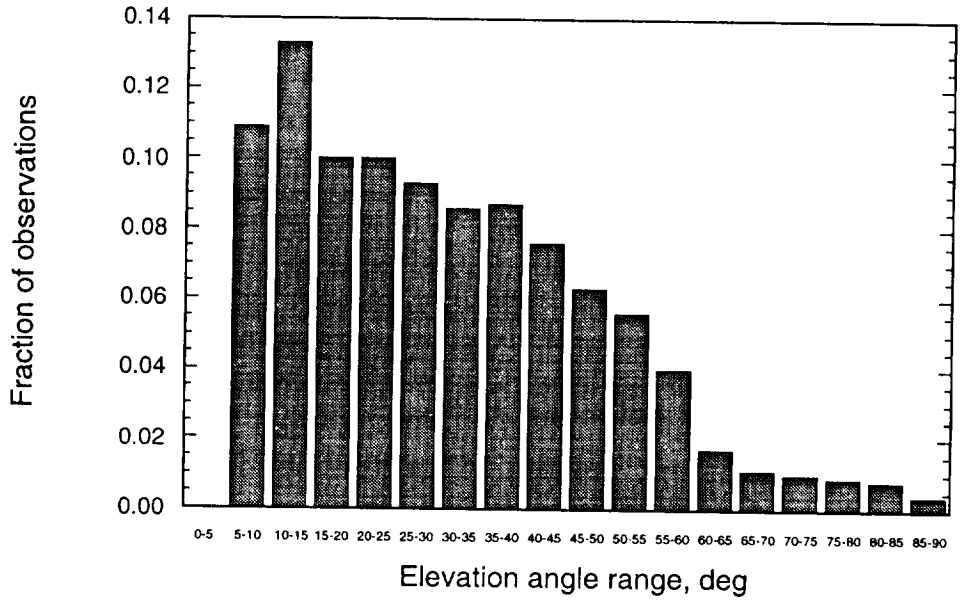

Figure 5. Histogram of elevation angle distributions of DSN Mark III VLBI observations.

The NMF function appears to show a performance nearly equivalent to that of the Lanyi mapping function, therefore, greater comparative detail is given here. Figure 6 shows the NMF minus Lanyi standard differences as a function of elevation angle. The two functions were evaluated at each station for all 11,897 observations. The results were placed in 0.5° bins for elevations lower than 20°, and 1° bins above 20°; the error bars in Fig. 6 correspond to the scatter from the average in each bin. The differences are as large as 3 cm just above 6° elevation, and decrease toward zero when approaching zenith.

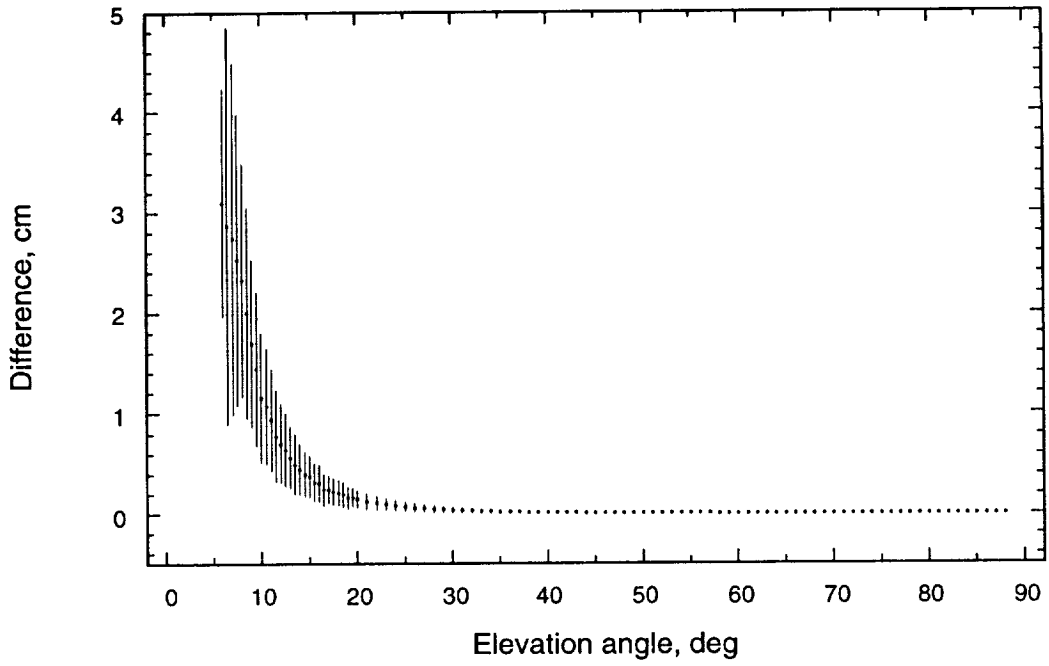

Figure 6. Tropospheric delay difference *vs.* elevation angle for DSN Mark III VLBI observations, NMF minus Lanyi mapping functions. (Each error bar is the standard deviation from the mean of all values in each elevation bin.)

5.3 Statistics of Post-fit Residuals

The post-fit quantities that were examined included the delay and delay rate residuals, the "baseline scatter" and chi square for a time-linear fit to baselines (estimated independently for each observing session), and the baseline length bias (change in baseline length at a given epoch induced by a change in the mapping function). Criteria for a good mapping function are small values for the residuals and the baseline scatter. Differences in the average angular dependence of the mapping functions, as well as in the resulting baseline scales, can point to particular elevation ranges or baselines which are not properly modeled.

Table 6 shows the RMS delay and delay rate residuals and total chi squares for the 10 VLBI fits. Normalized χ^2 values are not shown because of the uncertainty in partitioning parameters between the two observable types. The "improvement" columns in this table (as well as in Tables 7b and 8) contain the signed RMS difference between the residuals given by each mapping function and Lanyi standard. Focusing first on the residual results in Table 6, the mapping functions are seen to fall into three broad groups. Both Chao functions and the Chao tables produce fits to VLBI data that are definitely inferior, especially for delay rates. All other functions do not differ by more than a few picoseconds in delay residuals from the Lanyi function and its variants. Only the NMF and Ifadis functions, and Lanyi with parameters estimated, improve both the delay and delay rate residuals. As may be seen additionally from the

Table 6. Mark III VLBI residuals.

Mapping Function	Delay (τ) RMS (ps)	Delay (τ) χ^2	Delay rate ($\dot{\tau}$) RMS (fs/s)	Delay rate ($\dot{\tau}$) χ^2	Improvement Δ_τ (ps)	Improvement $\Delta_{\dot{\tau}}$ (fs/s)
1	71.6655	9665	131.512	13140	-19.4	-38.2
2	69.2402	8932	126.494	11883	-5.9	-12.7
3	70.4522	9176	154.737	21456	-14.3	-90.0
4	68.9867	8835	125.856	11701	. . .	. . .
5	69.0001	8838	125.869	11702	-1.4	-1.8
6	68.8222	8784	125.314	11599	+4.8	+12.7
7	69.0492	8844	126.315	11788	-2.9	-10.8
8	68.9374	8837	125.762	11717	+2.6	+4.9
9	69.0331	8838	125.767	11695	-2.5	+4.7
10	68.9273	8813	125.608	11682	+2.9	+9.4

subsequent results, the NMF and Ifadis functions show very similar behavior in all categories, and may be considered to be basically identical.

In order to assess the behavior of each tropospheric mapping function in various elevation angle ranges, the delay residuals were divided into six elevation bins in Tables 7a and 7b: below 10°, 5° bins up to 30°, and observations from 30° to zenith. Table 7a gives the raw results, while Table 7b relates them to the Lanyi standard function. It is seen that the NMF and Ifadis (and Lanyi with estimated parameters) improvement in residuals is not uniform across the range of elevations; they do well at very low angles, but not in the 10° to 15° and 25° to 30° ranges (this holds true for most of the newer functions). No extraordinary elevation-partitioned results are seen, with one exception: it can be noted that the Lanyi parameters-estimated function apparently achieves reductions in residuals by improving the mapping function "shape" at very low elevations.

Table 7a. Delay residuals (ps) by elevation angle.

Mapping Function	Range of Elevation Angles, deg 0–10	10–15	15–20	20–25	25–30	30–90
1	98.993	76.114	66.665	64.213	65.090	66.386
2	94.562	73.217	65.754	62.232	62.562	64.346
3	97.358	74.320	66.923	62.694	62.537	65.477
4	94.117	72.692	65.883	62.025	61.914	64.221
5	94.134	72.708	65.904	62.036	61.911	64.235
6	93.679	72.807	65.770	61.903	61.938	64.000
7	94.419	72.716	65.873	61.990	61.900	64.267
8	94.049	72.782	65.632	61.965	62.171	64.121
9	94.174	72.918	65.777	62.027	62.173	64.210
10	93.994	72.772	65.741	61.938	62.151	64.104

Table 7b. Improvement of delay residuals by elevation range.

Mapping Function	Improvement (ps) over Lanyi standard in quadrature					
	0–10	10–15	15–20	20–25	25–30	30–90
1	-30.7	-22.6	-10.2	-16.6	-20.1	-16.8
2	-9.2	-8.8	+4.1	-5.1	-9.0	-4.0
3	-24.9	-15.5	-11.8	-9.1	-8.8	-12.8
4	...	...	...	...	...	...
5	-1.8	-1.5	-1.7	-1.2	+0.6	-1.3
6	+9.1	-4.1	+3.9	+3.9	-1.7	+5.3
7	-7.5	-1.9	+1.1	+2.1	+1.3	-2.4
8	+3.6	-3.6	+5.7	+2.7	-5.6	+3.6
9	-3.3	-5.7	+3.7	-0.5	-5.7	+1.2
10	+4.8	-3.4	+4.3	+3.3	-5.4	+3.9

Table 8 shows baseline length results from the VLBI data analyses. It is seen that, without exception, any departure from the standard Lanyi mapping function increases the baseline scatter and χ^2 per degree of freedom (χ^2_ν) (with the exception of CfA-2.2 on the 15–65 baseline); sometimes by substantial amounts. The statistical significance of these differences can be inferred from the formal uncertainties of χ^2_ν. The number of degrees of freedom N in the California–Australia (15–45) and California–Spain (15–65) fits are 30 and 27, respectively. Thus $\sigma_{\chi^2_\nu} \approx (2/N)^{1/2} = 0.26$ and 0.27. Even for the best fits, however, χ^2_ν shows substantial departures from unity. This originates both from model inadequacies and from underestimated observable errors. It is assumed that the best fits correspond to the best modeling, and that in this case modeling errors and error underestimates contribute equally to the increased χ^2. Therefore the χ^2 value corresponding to the underestimated errors is $1 + (\chi^2 - 1)/2$. Consequently, in order to obtain a more realistic error for χ^2_ν, the formal $\sigma_{\chi^2_\nu}$ is multiplied by this estimated quantity; *i.e.*,

Table 8. Baseline length scatter (δ_B), improvement ($\Delta\delta_B$), and bias (β_B), mm.

Mapping Function	15–45		15–65		15–45		15–65	
	δ_B	χ^2_ν	δ_B	χ^2_ν	$\Delta\delta_B$	β_B	$\Delta\delta_B$	β_B
1	49.4	5.8	24.6	8.0	-40.8	173	-20.6	172
2	42.1	4.2	24.3	7.8	-31.5	90	-20.3	112
3	38.0	3.1	24.8	7.9	-25.8	26	-20.9	9
4	27.9	1.7	13.4	2.2	...	...	...	...
5	27.9	1.7	13.4	2.2	0.0	-3	0.0	-2
6	38.4	1.7	19.9	3.0	-26.4	6	-14.7	6
7	28.1	1.6	13.9	2.3	-3.3	20	-3.7	15
8	29.9	2.0	17.3	3.8	-10.8	62	-10.9	41
9	32.5	2.3	17.1	3.7	-16.7	61	-10.6	40
10	30.3	2.0	16.2	3.3	-11.8	58	-9.1	45

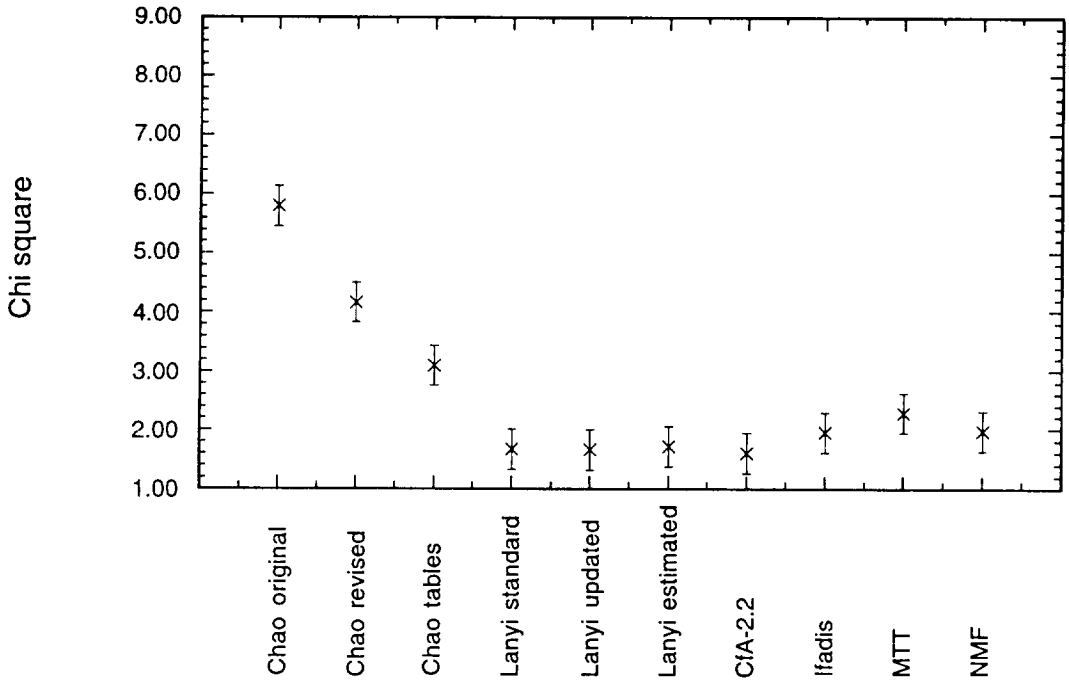

Figure 7a. Normalized χ^2 of residuals from a linear fit to baseline lengths *vs.* time for the California–Australia DSN baseline. (See text for explanation of error bars.)

1.3 and 1.6 for the two baselines, respectively. This gives $\sigma_{\chi_\nu^2} = 0.34$ and 0.44, which are the error bars used in Figs. 7a and 7b. Since all fits were based on identical data, the statistical difference between different solutions is the standard deviation of χ_ν^2 itself, *i.e.*, 0.34 or 0.44.

The differences are due to mapping errors and are seen to be highly significant for the group of three Chao functions *vs.* Lanyi. They are marginally significant for the remaining functions on the California–Australia baseline, and $> 2\sigma_{\chi_\nu^2}$ significant for Ifadis, MTT, and NMF *vs.* Lanyi on the California–Spain baseline. The Ifadis, MTT, and NMF mapping functions all worsen the scatter by at least 10 mm on both baselines. The CfA-2.2 function resembles Lanyi most closely in regard to scatter, and the two functions appear to be nearly identical. The Lanyi map with parameters estimated achieves its residual improvement at the expense of increases in baseline scatter of 26 and 15 mm. The purpose of this fit is to model any remaining variation in the mapping function; indeed, the RMS observable residuals decrease. This improvement appears to be achieved by propagating the delay residual errors into systematic baseline errors. The mechanism is poorly understood and is currently under further study. Most mapping functions also yield substantial baseline length biases relative to *Lanyi* [1984], ranging from 20 to 61 mm for the California–Australia 10,600-km baseline (the Chao tables do very well in this regard, only shifting the scale by 26 mm).

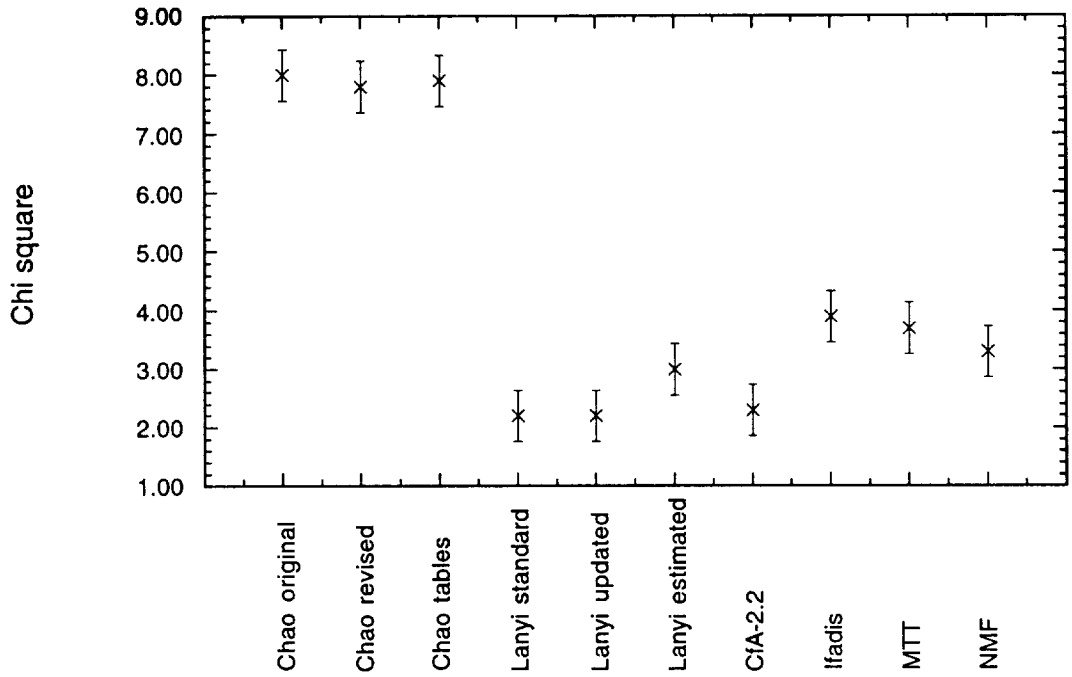

Figure 7b. Normalized χ^2 of residuals from a linear fit to baseline lengths *vs.* time for the California–Spain DSN baseline. (See text for explanation of error bars.)

5.4 Remarks

Based on the comparisons discussed in the previous subsections, a number of conclusions can be drawn. In the absence of more generalized testing, these should be regarded as limited to mapping the tropospheric delays at the three DSCCs. The statistical significance of differences among the mapping functions is tied to the residual scatter of these particular DSN VLBI fits. First, all three variants of the Chao mappings were very inadequate. They produced post-fit residual and baseline scatter values that were inferior by many cm relative to the more modern functions. Second, the 1984 Lanyi mapping function is still, by a small margin, equivalent or superior to all the newer algorithms developed during the intervening decade. Third, those mapping functions that employ limited or no surface meteorological data are either equivalent to or slightly worse than the Lanyi function. Some of their deficiencies may be due to the fact that their functional forms are based on atmospheric profiles measured at predominantly North American sites. Finally, of the functions using minimal or no surface data, either the Ifadis or NMF functions produce tropospheric calibration models of DSN VLBI measurements that are nearly equal in quality to those given by the Lanyi mapping function on the California–Australia baseline, but worse on the California–Spain baseline.

SECTION 6

SELECTION CRITERIA

There are number of selection criteria that can be used to determine whether or not a new or enhanced model should be incorporated into an institutional software set. For choice of a candidate tropospheric mapping function, the most immediately obvious selection criteria are (not necessarily in order of importance): 1) accuracy; 2) ease of implementation; 3) computational complexity, *i.e.*, processing time and memory requirements; 4) model complexity; 5) ease of use, *i.e.*, are surface weather data necessary or can standard inputs be overridden by the user; 6) experience base, or "maturity," of a particular model; and 7) "tuning" capability, *i.e.*, are partials available for estimated and "consider" parameters which can be adjusted.[3] In Table 9, an attempt is made to grossly categorize each of the candidate mapping functions against these seven selection criteria, each of which is discussed in greater detail below.

Table 9: Cursory rating of candidate tropospheric mapping functions against various selection criteria (on a scale of 1 to 4, where 1 is a low rating, and 4 is a high rating).

	Selection Criteria			
Mapping Function	Accuracy	Ease of Implementation[a]	Computational Complexity	Model Complexity
CfA-2.2	4 (≥ 5°)	3	3	4
Lanyi	4 (≥ 6°)	2	2	1
Ifadis	4 (≥ 2°)	3	3	4
MTT	4 (≥ 2°)	3	3	4
NMF	4 (≥ 3°)	4	3	3

	Ease of Use	Maturity	Tuning Capability
CfA-2.2	3	4	2
Lanyi	2	4	4
Ifadis	3	4	2
MTT	3	3	2
NMF	4	1	2

[a]ODP specific

[3]Consider parameters are an integral part of a "consider state analysis," a special case of reduced-order filtering theory used in orbit determination analysis. Various systematic error sources are treated as unmodeled parameters which are not estimated, but whose effects are accounted for (i.e., "considered") in computing the error covariance of the estimated parameters.

6.1 Accuracy

Although difficult to quantify, each candidate mapping function possesses a range of elevation angles and atmospheric profiles that demonstrates superior accuracy characteristics over its counterparts. Based on the accuracy assessment presented in the previous section, all of the candidate mapping functions demonstrate superior performance characteristics over the currently implemented Chao standard mapping tables and approximation formulas. A number of studies have been conducted within the past year or two that attempt to quantify the accuracy characteristics of various modern tropospheric mapping functions, including those presented in this report. For other recent VLBI-based results, see *MacMillan and Ma* [1994], and for recent GPS-based results, see *Mendes and Langley* [1993]. It should be noted that neither of these studies included the NMF mapping functions, as the studies preceded its release. However, the recent Mendes-Langley ray trace study does include the NMF functions [*Mendes and Langley*, 1994]. As this continues to be an active area research, and there is little doubt that by the time this report is printed, there will be a number of newly published reports that will give greater insight into the performance of today's highly accurate tropospheric mapping functions.

6.2 Ease of Implementation

Computer program mechanizations exist for all of the candidate mapping functions presented. Therefore, actual coding of the algorithms is not an implementation concern. The issue of accommodating a particular mapping function into the ODP's infrastructure is, however, a concern. Recall that the standard ODP tropospheric calibration model treats the dry and the wet components of the tropospheric adjustment separately. Therefore, with the exception of the Lanyi mapping function, any of the candidate dry and wet mapping functions could easily be incorporated into the ODP tropospheric adjusts model simply by replacing ELVFAC in Eq. (9) with the appropriate procedural call. Because all of the candidate mapping functions (with the exception of NMF) have provision for specifying real-time surface meteorological data, further ODP modifications would have to be made in order to accommodate these additional inputs. This would most likely be accomplished in the form of additional inputs on the General INputs (GIN) file. Such a requirement is necessary not only for the computations of the actual corrections to the modeled observables, but also for the computations of the parameter partials that the user may wish to adjust. Therefore, both the EDIT and REGRES program links would be impacted. In addition, the Lanyi, MTT, and NMF mapping functions all utilize the site-dependent parameters of geodetic station latitude and height. Therefore, procedural calls to special utility libraries would have to be made in both program links in order to convert the station coordinates given in the conventional spherical or cylindrical coordinates relative to the prime meridian, equator, and mean pole of 1903.0 to geodetic station coordinates. Finally, the NMF dry mapping function requires the day-of-year (DOY) as a functional input; thus, an appropriate time conversion would be necessary to convert the time past epoch from the current ODP time format to DOY.

6.3 Computational Complexity

Because high-speed workstation computers are readily accessible in the work center today, computational limitations with respect to the different candidate mapping functions are not a concern, at least not for tracking and navigation operations at JPL. As an example, the processing of several thousand data points that were analyzed in the DSN Mark III VLBI accuracy assessment was performed with no appreciable difference between mapping functions in terms of processing time or memory requirements. Therefore, no attempt was made to benchmark the various candidate mapping functions for time and space complexity on different computer platforms. A cursory examination of the processing time requirements for these and several other mapping functions (including Chao's original approximation formula) is presented in *Mendes and Langley* [1993]. Results from that study suggested that for certain computational platforms, the Lanyi mapping function's computational requirements were significantly greater than the other mapping functions evaluated.

6.4 Model Complexity

The level of mathematical sophistication or complexity of a proposed model may be targeted as one of the critical criteria of choice over another candidate model. For the majority of analysts who would invoke a selectable tropospheric calibration model in the ODP, the level of complexity of the underlying model is generally not an issue. Users are typically more concerned with the model's ease of use rather than its mathematical sophistication, as long as the model has been proven to yield improved results over the former model. In contrast, if an analyst wishes to make modifications or enhancements to a newly incorporated model, the issue of model complexity becomes much more important. Upon review of the mathematical formulations of the candidate tropospheric mapping functions presented in this report (*cf.*, Section 4), it is clear that the Lanyi model is by far the most complex, as it was derived analytically. Although the input parameterizations vary significantly between the CfA-2.2, Ifadis, and MTT semi-empirical models, all are relatively straightforward and similar in format. The NMF model, although somewhat more sophisticated in its parameterizations of the mapping coefficients than the other empirically based models, is still relatively straightforward in its formulation.

6.5 Ease of Use

Another important factor in the selection process of a proposed model upgrade, and somewhat related to model complexity, is how easy it is to use. In the current ODP implementation of the tropospheric mapping phase, minimal input is required of the user in order to utilize the Chao dry (TABDRY) and wet (TABWET) standard mapping tables for data editing, and the Chao dry and wet approximation formulas for the parameter partials. Although the capability for overriding the TABDRY and TABWET arrays has existed for over 2 decades, this option has yet to be exercised. Because the majority of the candidate mapping functions support surface meteorological parameters, there is a trade-off between the potential for greater accuracy

and the additional requirement on the user to maintain much greater attention to detail. Standard or default values for the surface meteorological parameters could be used for routine applications, resulting in less accuracy, but with reduced burden on the user. Because the NMF dry and wet mapping functions do not rely on input surface meteorological parameters, they are clearly the easiest mapping functions to use, with all inputs transparent to the user.

6.6 Maturity

The experience base, or "maturity," of a particular model must also be considered in the evaluation process. The Lanyi mapping function has been used extensively at JPL for precision VLBI- and GPS-based analysis since its pre-release in 1983, while the CfA-2.2 dry mapping function of Davis et al. has also seen extensive use, principally by the U.S. East Coast and international geodetic science activities, since the mid-1980s. The MTT mapping functions, apparently intended to supersede the CfA-2.2, were published in 1992 and have also seen extensive use in high-precision geodetic applications. The global Ifadis mapping functions, although introduced as early as 1986, do not appear to have been as actively "marketed" as some of the other candidate mapping functions presented [*McCarthy*, 1992]; nevertheless, their performance in the precision applications has thus far has been commendable, yielding results comparable to or better than the MTT mapping functions. The NMF mapping functions are clearly the "new kid on the block," and as such, do not possess the level of maturity seen for the other candidate mapping functions. However, preliminary analysis against ray traces based on radiosonde profile data [*Mendes and Langley*, 1994] and experimental evaluation using VLBI measurements (*cf.*, Section 5), suggests accuracy levels as good or better than the Ifadis and MTT mapping functions.

6.7 Tuning Capability

The final selection criteria suggested herein regards a candidate model's "tuning" capability, *i.e.*, the capability of a particular model to support parameters which can be adjusted in the data filtering or estimation process. More specifically, partials are available for parameters which can either be estimated or treated as unmodeled "consider" parameters. The most commonly utilized error model parameter partials for the tropospheric calibration model are with respect to zenith dry and wet delays [*cf.*, Eqs. (21) and (22)]. In an effort to further improve the parameter estimation process, the mapping coefficients given by the CfA-2.2, Ifadis, MTT, and NMF mapping functions could be promoted to estimable parameters, as was done for Chao's original semi-empirical dry mapping function in JPL's VLBI parameter estimation software set, MODEST [*Sovers and Jacobs*, 1994]. Currently, only the Lanyi mapping function supports an additional tuning parameter to account for the absence of real-time surface meteorological data. Recall that in the reduction of DSN Mark III VLBI measurements (discussed in Section 5), use of this additional tuning parameter resulted in improved post-fit residuals, albeit at the expense of increased baseline scatter.

SECTION 7

SUMMARY AND CONCLUSIONS

The current implementation of the ODP's standard tropospheric calibration model was reviewed in extensive detail. The standard model is an adaptation of the seasonal model developed by C. C. Chao in the early 1970s to support the Mariner Mars 1971 program, and has seen only modest changes since it was incorporated into the ODP. As part of a model upgrade effort, this report reviewed the format and content of the zenith delay tropospheric calibrations supplied by the DSN's TSAC activity, as well as the tropospheric mapping process, whereby the zenith delay calibrations are projected along the station-to-spacecraft line of sight. All mathematical descriptions of the standard model were presented, along with ODP program link interface requirements. Proposed improvements to the current model were described for both the zenith delay calibration and zenith delay mapping processes.

The proposed improvements for the zenith delay calibration process are currently under review by TSAC, and include calibrations based on real-time surface meteorological measurements, as well as calibrations derived from GPS ground-based observations. The principal focus of this report was to review a set of relatively new models in an effort to modernize the current zenith delay mapping process. These new models, or "tropospheric mapping functions," are accurate over a wide range of observer-to-radio source elevation angles. Moreover, nearly all of the newer mapping functions have been used successfully in a variety of high-precision geodetic experiments. Candidate mapping functions of Lanyi, Davis et al. (CfA-2.2), Ifadis (global solution model), Herring (MTT), and the recent Niell (NMF) mapping functions were described. All of the candidate mapping functions demonstrated superior accuracy characteristics over the currently implemented Chao model, which takes the form of standard mapping tables derived from early ray trace calculations and simple approximation formulas to perform the mapping. These performance results were based on a statistical analysis of DSN Mark III VLBI measurements acquired over a 5-year period from 1988 to 1993.

Clearly, no one "best" tropospheric mapping function exists for every application and all ranges of elevation angles; however, based on the comparative survey presented, the authors recommend that the Lanyi and NMF mapping functions be incorporated into the ODP as user-selectable options, in addition to the currently implemented Chao model.

Justification for this recommendation follows:

1) Although the Lanyi model would admittedly be the most difficult to incorporate into the ODP's current media calibration infrastructure, it has the advantage of being adaptable to a wide variety of atmospheric conditions, given the provisions to input real-time weather data. In the accuracy analysis presented, the Lanyi mapping function was seen to be superior over its counterparts–the CfA-2.2, Ifadis, MTT, and NMF functions–at 6° elevation or higher.

Furthermore, the CfA-2.2 lacks a companion model for the wet atmospheric component. A cursory examination was made of the sensitivity of the Lanyi mapping function to variations in surface meteorological data. However, the level of accuracy given by the DSN's surface instruments has yet to be determined and will require further investigation; standard (average) values for the weather data can be used in the interim that will still yield high-fidelity results. Another argument for implementing the Lanyi model is that line-of-sight tropospheric delay predictions as measured by the GPS ground system are typically mapped to the zenith direction in time series format using Lanyi's mapping function. Therefore, the Lanyi model would have to be an available option in the ODP in order to support any future GPS-based zenith delay calibrations provided by TSAC; otherwise, post-fit results will be biased if a different mapping function is used to "de-map" the zenith delays. The final argument given here for implementing the Lanyi mapping function is that for most applications supported by the DSN, the Lanyi mapping function is expected to perform as well or better than the other candidate models at 6° elevation angle and above; recall that operational constraints of the DSN radio antennas usually preclude tracking below 6°. For non-DSN applications that require tracking significantly below this level, the Ifadis, MTT, or NMF mapping functions are recommended.

2) The NMF model, although lacking maturity, has the advantage of performing as well as or better than its counterparts, such as the Ifadis or MTT models, without requiring surface meteorological input data. Therefore, ODP users would not be burdened with specific model interfaces. It appears that the NMF mapping functions will gain popularity over time, since they are easy to use and have been shown to be highly accurate over a wide range of elevation angles in certain experimental applications. In addition, the NMF mapping functions utilize the same form of the Marini continued fraction as Ifadis and MTT (truncated at three terms in the expansion), the principal difference being in the parameterizations of the mapping function coefficients. Thus, an argument can be made that the NMF model will eventually supersede the Ifadis and MTT models.

3) The Chao model should remain as the default option, at least in the near term. It would be imprudent to suggest replacing the Chao model in its entirety, as orbit determination analysts frequently attempt to reconstruct "old" data and validate anomalies encountered during past mission operations. In addition, the ODP is a "flight-certified" software set; thus, any proposed modeling improvements would have to be rigorously tested against the original standard model before they could be accepted as a new standard.

In closing, recall that all of the candidate mapping functions were derived under the assumption of a spherically symmetric atmosphere. Except for ultra-high-precision applications, this azimuthal asymmetry assumption is typically adequate. Consequently, for routine support of flight operations, such a level of model sophistication does not yet seem warranted, at least not for ODP implementation. The interested reader is referred to publications by *Gardner* [1977] and *Wilcox* [1994] for examples of novel solutions to the azimuthal asymmetry problem.

REFERENCES

Baby, H. B., P. Golé, and J. Lavergnat, "A Model for the Tropospheric Excess Path Length of Radio Waves from Surface Meteorological Measurements," *Radio Science*, Vol. 23, No. 6, pp. 1023-1038, 1988.

Bean, B. R., and E. J. Dutton, *Radio Meteorology*, Monograph 92, National Bureau of Standards, Washington, D. C., pp. 1-44, 1966.

Berman, A. L., "A New Tropospheric Range Refraction Model," *Space Programs Summary 37-65*, Vol. II, pp. 140-153, Jet Propulsion Laboratory, Pasadena, California, September 30, 1970.

Berman, A. L., "The Prediction of Zenith Range Refraction from Surface Measurements of Meteorological Parameters," *JPL Technical Report 32-1602*, Jet Propulsion Laboratory, Pasadena, California, July 15, 1976.

Callahan, P. S., "Prediction of Tropospheric Wet Component Range Error From Surface Measurements," *The DSN Progress Report for September and October 1973*, Technical Report 32-1526, Vol. XVIII, Jet Propulsion Laboratory, Pasadena, California, pp. 41-46, December 15, 1973.

Chao, C. C., "A Preliminary Estimation of Tropospheric Influence on the Range and Range Rate Data During the Closest Approach of the MM'71 Mars Mission," JPL Technical Memorandum 391-129 (internal document), Jet Propulsion Laboratory, Pasadena, California, October 21, 1970.

Chao, C. C., "New Tropospheric Range Corrections with Seasonal Adjustment," *The DSN Progress Report For September and October 1971*, Technical Report 32-1526, Vol. VI, Jet Propulsion Laboratory, Pasadena, California, pp. 67-82, December 15, 1971.

Chao, C. C., "A Model for Tropospheric Calibration from Daily Surface and Radiosonde Balloon Measurement," JPL Technical Memorandum 391-350 (internal document), Jet Propulsion Laboratory, Pasadena, California, August 8, 1972*a*.

Chao, C. C., "Improved Tropospheric Mapping Tables (Including Bending Effect) for SATODP," JPL Interoffice Memorandum 391.3-637 (internal document), Jet Propulsion Laboratory, Pasadena, California, December 28, 1972*b*.

Chao, C. C., "New Method to Predict Wet Zenith Range Correction From Surface Weather Measurements," *The DSN Progress Report*, Technical Report 32-1526, Vol. XIV, Jet Propulsion Laboratory, Pasadena, California, pp. 33-41, April 15, 1973.

Chao, C. C., "The Tropospheric Calibration Model for Mariner Mars 1971," *JPL Technical Report 32-1587*, Jet Propulsion Laboratory, Pasadena, California, pp. 61-76, March, 15, 1974.

Chao, C. C. (private communication), The Aerospace Corporation, El Segundo, California, March 23, 1994.

Christensen, C. S., "Troposphere and Charge Particle Adjustments in the ODP," JPL Interoffice Memorandum 314.5-296 (internal document), Jet Propulsion Laboratory, Pasadena, California, March 2, 1979*a*.

Christensen, C. S., "On the Elevation Angle and its use for WEIGHT and DELETE in the ODP," JPL Interoffice Memorandum 314.5-298 (internal document), Jet Propulsion Laboratory, Pasadena, California, March 12, 1979*b*.

Collier, J. B., "CSP System User's Guide," unpublished manuscript, Jet Propulsion Laboratory, Pasadena, California, February 4, 1981.

Collier, J. B. (private communication), Navigation Systems Section, Jet Propulsion Laboratory, Pasadena, California, June 13, 1993.

Davis, J. L., T. A. Herring, I. I. Shapiro, A. E. E. Rogers, and G. Elgered, "Geodesy by Radio Interferometry: Effects of Atmospheric Modeling Errors on Estimated Baseline Length," *Radio Science*, Vol. 20, No. 6, pp. 1593-1607, 1985.

DPTRAJ-ODP User's Reference Manual, Vol. 1, Rev. F, JPL Internal Document D-263, Jet Propulsion Laboratory, Pasadena, California, pp. 282-308 and pp. 469-471, June 28, 1994.

DSN Tracking System Interfaces, Media Calibration Interface (TRK-2-23), DSN System Requirements Detailed Interface Design, JPL Internal Document 820-13; Rev. A, April 19, 1985.

Ekelund, J. E. (private communication), Navigation Systems Section, Jet Propulsion Laboratory, Pasadena, California, August 4, 1993.

Elgered, G., J. L. Davis, T. A. Herring, and I. I. Shapiro, "Geodesy by Radio Interferometry: Water Vapor Radiometry for Estimation of Wet Delay," *Journal of Geophysical Research*, Vol. 96, No. B4, pp. 6541-6555, 1991.

Elgered, G., "Tropospheric Radio Path Delay from Ground-Based Microwave Radiometry," *Atmospheric Remote Sensing by Microwave Radiometry*, M. A. Janssen, ed., New York: John Wiley & Sons, pp. 219-221, 1993.

Gallini, T. E., "A Survey of Tropospheric Refraction Models," *Aerospace Report No. TOR-94(4488)-11*, The Aerospace Corporation, El Segundo, California, April 20, 1994.

Gardner, C. S., "Correction of Laser Tracking Data for the Effects of Horizontal Refractivity Gradients," *Applied Optics*, Vol. 16, No. 9, pp. 2427-2432, 1977.

Herring, T. A., J. L. Davis, and I. I. Shapiro, "Geodesy by Radio Interferometry: The Application of Kalman Filtering to the Analysis of VLBI Data," *Journal of Geophysical Research*, Vol. 95, No. B8, pp. 12561-12581, 1990.

Herring, T. A., "Modeling Atmospheric Delays in the Analysis of Space Geodetic Data," *Proceedings of Refraction of Transatmospheric Signals in Geodesy*, Netherlands Geodetic Commission Series No. 36, The Hague, Netherlands, pp. 157-164, May 19-22, 1992.

Hopfield, H. S., "Tropospheric Effect on Electromagnetically Measured Range: Prediction from Surface Weather Data," *Radio Science*, Vol. 6, No. 3, pp. 357-367, 1971.

Ifadis, I. I., "The Atmospheric Delay of Radio Waves: Modeling the Elevation Dependence on a Global Scale," *Technical Report No. 38L*, Chalmers University of Technology, Göteborg, Sweden, 1986.

Lanyi, G. E., "Tropospheric Propagation Delay Effects for Radio Waves," JPL Interoffice Memorandum 335.1-156 (internal document), Jet Propulsion Laboratory, Pasadena, California, November 15, 1983.

Lanyi, G., "Tropospheric Delay Effects in Radio Interferometry," *The TDA Progress Report 42-78*, Vol. April–June 1984, Jet Propulsion Laboratory, Pasadena, California, pp. 152-159, August 15, 1984.

Lanyi, G. E. (private communication), Tracking Systems and Applications Section, Jet Propulsion Laboratory, September 1993.

Lichten, S. M. (private communication), Tracking Systems and Applications Section, Jet Propulsion Laboratory, Pasadena, California, June 24, 1994.

MacMillan, D. S., and C. Ma, "Evaluation of Very Long Baseline Interferometry Atmospheric Modeling Improvements," *Journal of Geophysical Research*, Vol. 99, No. B1, pp. 637-651, 1994.

MacMillan, D. S. (private communication), NVI Incorporated and Goddard Space Flight Center, Greenbelt, Maryland, June 22, 1994.

Marini, J. W., "Correction of Satellite Tracking Data for an Arbitrary Tropospheric Profile," *Radio Science*, Vol. 7, No. 2, pp. 223-231, 1972.

McCarthy, D. D. (ed.), "IERS Standards (1992)," *IERS Technical Note 13*, Central Bureau of IERS–Observatoire de Paris, pp. 116-120, July 1992.

Mendes, V. B., and R. B. Langley, "Application of the Global Positioning System to the Assessment of Crustal Deformation in the Charlevoix Seismic Zone," *Proceedings of ION GPS-93*, Vol. II, Sixth International Technical Meeting of the Satellite Division of The Institute of Navigation, Salt Lake City, Utah, pp. 1205-1219, September 22-24, 1993.

Mendes, V. B., and R. B. Langley, "A Comprehensive Analysis of Mapping Functions Used in Modeling Tropospheric Propagation Delay in Space Geodetic Data," paper presented at KIS94, International Symposium on Kinematic Systems in Geodesy, Geomatics and Navigation, Banff, Canada, August 30–September 2, 1994.

Miller, L. F., V. J. Ondrasik, and C. C. Chao, "A Cursory Examination of the Sensitivity of the Tropospheric Range and Doppler Effects to the Shape of the Refractivity Profile," *The DSN Progress Report*, Technical Report 32-1526, Vol. I, Jet Propulsion Laboratory, Pasadena, California, pp. 22-30, February 15, 1971.

Mottinger, N. A., "Reflections on Refraction—A Historical Overview of the Tropospheric Refraction Model in the ODP," JPL Interoffice Memorandum 314.10-385 (internal document), Jet Propulsion Laboratory, Pasadena, California, January 18, 1984.

Moyer, T. D., "Solid Earth Tides and Analytic Partials for Troposphere and Ionosphere Parameters in Link Regres for Galileo," JPL Interoffice Memorandum 314.5-786 (internal document), Jet Propulsion Laboratory, Pasadena, California, May 17, 1984

Niell, A. E., "A New Approach for the Hydrostatic Mapping Function," *Proceedings of the International Workshop for Reference Frame Establishment and Technology Development in Space Geodesy*, Communications Research Laboratory, Koganei, Tokyo, Japan, pp. 61-68, January 1993.

Niell, A. E. (electronic mail message), "New mapping functions good to 3 degrees," MIT Haystack Observatory, Westford, Massachusetts, January 26, 1994*a*.

Niell, A. E., "Global Mapping Functions for the Atmospheric Delay at Radio Wavelengths," (report in preparation), 1994*b*.

Ondrasik, V. J., "Tables for Mapping Tropospheric and Ionospheric Zenith Range Effects Down to Lower Elevation Angles," JPL Interoffice Memorandum 391.2-116 (internal document), Jet Propulsion Laboratory, Pasadena, California, December 28, 1970.

Panagiotacopulos, N. D., J. W. Zielenbach, and R. W. Duesing, "An Introduction to JPL's Orbit Determination Program," *JPL Publication 1846-37*, Jet Propulsion Laboratory, Pasadena, California, May 21, 1974.

Resch, G. M., "Water Vapor Radiometry in Geodetic Applications," *Geodetic Refraction*, F. K. Brunner, ed., Springer-Verlag, New York, 1984.

Royden, H. N. (private communication), Tracking Systems and Applications Section, Jet Propulsion Laboratory, Pasadena, California, May 19, 1994.

Runge, T. F., "Troposphere Calibration Software," *TDA/DSN Document No. SRD-NVI-5454-OP Rev. A*, Jet Propulsion Laboratory, Pasadena, California, August 31, 1993.

Runge, T. F. (private communication), Tracking Systems and Applications Section, Jet Propulsion Laboratory, Pasadena, California, June 16, 1994.

Saastamoinen, J., "Atmospheric Correction for The Troposphere and Stratosphere in Radio Ranging of Satellites," *The Use of Artificial Satellites for Geodesy, Geophysical Monograph 15*, S. W. Henrikson et al., eds., pp. 247-251, American Geophysical Union, Washington, D.C., 1972.

Smith, M. A., "Analysis of Meteorological Balloon Data," JPL Interoffice Memorandum 335.6-92-023 (internal document), Jet Propulsion Laboratory, Pasadena, California, July 27, 1992.

Sovers, O. J., C. D. Edwards, C. S. Jacobs, G. E. Lanyi, K. M. Liewer, and R. N. Treuhaft, "Astrometric Results of 1978-1985 Deep Space Network Radio Interferometry: The JPL 1987-1 Extragalactic Source Catalog," *Astronomical Journal*, Vol. 95, pp. 1647-1658, 1988.

Sovers, O. J., "JPL 1990-3: A 5-nrad Extragalactic Source Catalog Based on Combined Radio Interferometric Observations," *The TDA Progress Report 42-106*, Vol. April–May 1991, Jet Propulsion Laboratory, Pasadena, California, pp. 364-383, August 15, 1991.

Sovers, O. J., and C. S. Jacobs, "Observation Model and Parameter Partials for the JPL VLBI Parameter Estimation Software "MODEST"—1994," *JPL Publication 83-39, Rev. 5*, Jet Propulsion Laboratory, Pasadena, California, pp. 58-61, August 1994

Sovers, O. J., and G. E. Lanyi, "Evaluation of Current Tropospheric Mapping Functions by Deep Space Network Very Long Baseline Interferometry," *The TDA Progress Report 42-119* (in press), Vol. July–September 1994, Jet Propulsion Laboratory, Pasadena, California, November 15, 1994.

Thayer, G. D., "An Improved Equation for the Radio Refractive Index of Air," *Radio Science*, Vol. 9, No.10, pp. 803-807, 1974.

Tralli, D. M., and S. M. Lichten, "Stochastic Estimation of Tropospheric Path Delays in Global Positioning System Geodetic Measurements," *Bulletin Geodesique*, Vol. 64, pp. 127-159, 1990.

Tralli, D. M., S. M. Lichten, and T. A. Herring, "Comparison of Kalman Filter Estimates of Zenith Atmospheric Path Delays Using the Global Positioning System and Very Long Baseline Interferometry," *Radio Science*, Vol. 27, No. 6, pp. 999-1007, 1992.

Ulvestad, J. S., and S. W. Thurman, "Orbit-Determination Performance of Doppler Data for Interplanetary Cruise Trajectories Part I: Error Analysis Methodology," *The TDA Progress Report 42-108*, Vol. October–December 1991, Jet Propulsion Laboratory, Pasadena, California, pp. 31-48, February 15, 1992.

Ulvestad, J. S., "Orbit-Determination Performance of Doppler Data for Interplanetary Cruise Trajectories Part II: 8.4-GHz Performance and Data-Weighting Strategies," *The TDA Progress Report 42-108*, Vol. October–December 1991, Jet Propulsion Laboratory, Pasadena, California, pp. 49-65, February 15, 1992.

Wilcox, J. Z., "The Effect of Tropospheric Fluctuations on the Accuracy of Water Vapor Radiometry," *The TDA Progress Report 42-110*, Vol. April–June 1992, Jet Propulsion Laboratory, Pasadena, California, pp. 33-51, August 15, 1992.

Wilcox, J. Z., "Line-of-Sight Tropospheric Calibration from Measurements in Arbitrary Directions," *The TDA Progress Report 42-116*, Vol. October–December 1993, Jet Propulsion Laboratory, Pasadena, California, pp. 10-23, February 15, 1994.

Winn, F. B., S. C. Wu, G. M. Resch, C. C. Chao, O. H. von Roos, and H. S. Lau, "Atmospheric Water Vapor Calibrations: Radiometer Technique," *The DSN Progress Report 42-32*, Vol. January and February 1976, Jet Propulsion Laboratory, Pasadena, California, pp. 38-49, April 15, 1976.

APPENDIX

Chao's Latest Wet (TABWET) and Dry (TABDRY) Standard Mapping Tables

```
$$$$$$$$$$$$$$$$$$$$$$$$$$$$$$$$$$$$$$$$$$$$$$$$$$$$$$$$$$$$$$$$$$$$$$$$$$$$$$$$$
$
$  TABWET and TABDRY from C.C. Chao 8/29/77
$
$   The elevation angle (in degrees) corresponding to each TAB
$   value lies above it in the table.
$
$  43) Mottinger, N.A., "Reflections on Refraction -- A Historical
$       Overview of the Tropospheric Refraction Model in the ODP,"
$       IOM 314.10-385, January 18,  1984.
$
$  44) Chao, C.C., "Improved Tropospheric Mapping Tables
$       (Including Bending Effect) for SATODP," IOM 391.3-637,
$       December 28, 1972.
$
$  45) Chao, C.C., "Improved Estimation of the Parameters and Mapping
$       Tables of Tropospheric Calibration for MM71," IOM 391.3-352,
$       May 25,1971.
$
  TABWET(1)=261*0.,
$
  TABWET(1)=
 $     .00
     61.5790,
 $     .10      .20      .30      .40      .50      .60      .70      .80      .90   ,
     57.8413,54.3927,51.2432,48.3625,45.7235,43.3021,41.0769,39.0284,37.1397,
 $    1.00     1.10     1.20     1.30     1.40     1.50     1.60     1.70     1.80   ,
     35.3955,33.7820,32.2870,30.8996,29.6100,28.4095,27.2901,26.2449,25.2675,
 $    1.90     2.00     2.10     2.20     2.30     2.40     2.50     2.60     2.70   ,
     24.3521,23.4935,22.6873,21.9291,21.2152,20.5420,19.9066,19.3060,18.7377,
 $    2.80     2.90     3.00     3.10     3.20     3.30     3.40     3.50     3.60   ,
     18.1994,17.6889,17.2042,16.7435,16.3053,15.8880,15.4903,15.1108,14.7484,
 $    3.70     3.80     3.90     4.00     4.10     4.20     4.30     4.40     4.50   ,
     14.4021,14.0709,13.7538,13.4500,13.1587,12.8792,12.6109,12.3530,12.1051,
 $    4.60     4.70     4.80     4.90     5.00     5.10     5.20     5.30     5.40   ,
     11.8666,11.6369,11.4157,11.2024,10.9967,10.7982,10.6065,10.4213,10.2423,
 $    5.50     5.60     5.70     5.80     5.90     6.00     6.10     6.20     6.30   ,
     10.0692, 9.9017, 9.7395, 9.5824, 9.4302, 9.2827, 9.1396, 9.0008, 8.8660,
 $    6.40     6.50     6.60     6.70     6.80     6.90     7.00     7.10     7.20   ,
      8.7352, 8.6081, 8.4845, 8.3645, 8.2477, 8.1341, 8.0235, 7.9159, 7.8111,
 $    7.30     7.40     7.50     7.60     7.70     7.80     7.90     8.00     8.10   ,
      7.7090, 7.6094, 7.5125, 7.4179, 7.3256, 7.2356, 7.1478, 7.0621, 6.9784,
 $    8.20     8.30     8.40     8.50     8.60     8.70     8.80     8.90     9.00   ,
      6.8966, 6.8167, 6.7387, 6.6624, 6.5878, 6.5148, 6.4435, 6.3737, 6.3054,
 $    9.10     9.20     9.30     9.40     9.50     9.60     9.70     9.80     9.90   ,
      6.2385, 6.1730, 6.1089, 6.0462, 5.9847, 5.9244, 5.8653, 5.8075, 5.7507,
 $   10.00    10.50    11.00    11.50    12.00    12.50    13.00    13.50    14.00   ,
      5.6951, 5.4323, 5.1929, 4.9739, 4.7728, 4.5876, 4.4164, 4.2578, 4.1104,
 $   14.50    15.00    15.50    16.00    16.50    17.00    17.50    18.00    18.50   ,
      3.9731, 3.8449, 3.7250, 3.6125, 3.5069, 3.4075, 3.3138, 3.2253, 3.1417,
 $   19.00    19.50    20.00    20.50    21.00    21.50    22.00    22.50    23.00   ,
      3.0625, 2.9874, 2.9160, 2.8483, 2.7838, 2.7223, 2.6637, 2.6078, 2.5543,
```

TECHNICAL REPORT STANDARD TITLE PAGE

1. Report No. 94-24	2. Government Accession No.	3. Recipient's Catalog No.
4. Title and Subtitle: A Comparative Survey of Current and Proposed Tropospheric Refraction-Delay Models for DSN Radio Metric Data Calibration		5. Report Date: October 1994 6. Performing Organization Code
7. Author(s): J. A. Estefan and O. J. Sovers		8. Performing Organization Report No.
9. Performing Organization Name and Address: JET PROPULSION LABORATORY, California Institute of Technology, 4800 Oak Grove Drive, Pasadena, California 91109		10. Work Unit No. 11. Contract or Grant No. NAS7-918 13. Type of Report and Period Covered: Survey and evaluation
12. Sponsoring Agency Name and Address: NATIONAL AERONAUTICS AND SPACE ADMINISTRATION, Washington, D.C. 20546		14. Sponsoring Agency Code BG31430116002

15. Supplementary Notes

16. Abstract

The standard tropospheric calibration model implemented in the operational Orbit Determination Program is the seasonal model developed by C. C. Chao in the early 1970s. The seasonal model has seen only slight modification since its release, particularly in the format and content of the zenith delay calibrations. Chao's most recent standard mapping tables, which are used to project the zenith delay calibrations along the station-to-spacecraft line of sight, have not been modified since they were first published in late 1972. This report focuses principally on proposed upgrades to the zenith delay mapping process, although modeling improvements to the zenith delay calibration process are also discussed. A number of candidate approximation models for the tropospheric mapping are evaluated, including the semi-analytic mapping function of Lanyi, and the semi-empirical mapping functions of Davis et al. ("CfA-2.2"), of Ifadis (global solution model), of Herring ("MTT"), and of Niell ("NMF"). All of the candidate mapping functions are superior to the Chao standard mapping tables and approximation formulas when evaluated against the current Deep Space Network Mark III intercontinental very long baseline interferometry database.

17. Key Words (Selected by Author(s))	18. Distribution Statement
tropospheric antenna calibration; zenith delay mapping; Deep Space Network	

19. Security Classif. (of this report)	20. Security Classif. (of this page)	21. No. of Pages	22. Price
Unclassified	Unclassifed	53	